UiT
THE ARCTIC
UNIVERSITY
OF NORWAY

Faculty of Science and Technology, Department of Physics and Technology

The Cretaceous development of the Nordkapp Basin based on seismic interpretation

—

Aleksei Matveev

EOM-3901 Master's Thesis in Energy, Climate and Environment, 30 ECTS
May 2018

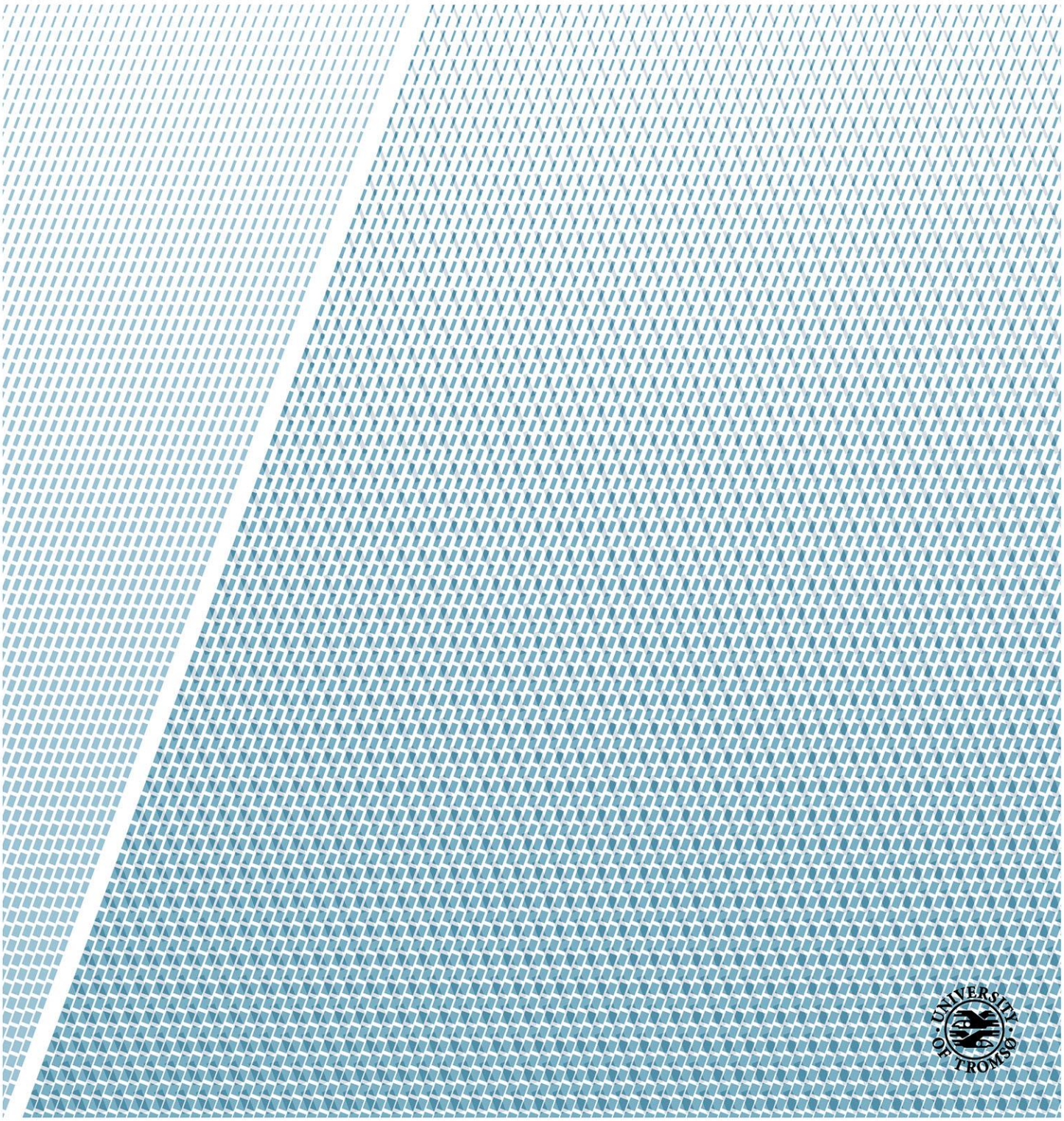

UiT / THE ARCTIC UNIVERSITY OF NORWAY

The Cretaceous development of the Nordkapp Basin based on seismic interpretation

Faculty of Science and Technology

Department of Physics and Technology

Aleksei Matveev

EOM-3901 Master's Thesis in Energy, Climate and Environment

30 ECTS

May 2018

Abstract

This thesis is focused on studying the development of the Nordkapp Basin during the Cretaceous Period. The basin is fault-controlled and is strongly influenced by salt tectonics. The basin is divided into two parts, which differs both in the average width and direction of their elongation. Moreover, the salt structures in the northeast and southwest parts of the basin also follow the trends in width and direction.

During the Early Cretaceous, the thick sequences of terrestrial sediments were deposited in the basin. Fault development and salt activity remained inactive during the Cretaceous Period, which opened the window for shelf progradation along the basin from northeast to southwest. Progradation also followed the overall regional trend, and the regional evolution of the Barents Sea directly influenced the basin as tectonic events triggered fault development and salt movements. Moreover, this also led to changes in sediment supply.

The numerous 2D seismic surveys of the Southwest Barents Sea are studied in this thesis. Four reflectors are interpreted and three 3D surfaces are made. Correlation of seismic and well data helped to understand the time of deposition of the interpreted surfaces. The time-thickness maps are also made and studied in the thesis. Analysis of all the 3D surfaces helped to understand and discuss the depositional environment in the Nordkapp Basin during the Cretaceous Period. The timing of the second phase of the salt activity is also discussed.

Acknowledgements

I would like to express my gratitude to my principal supervisor Stig-Morten Knutsen and co-supervisor Iver Martens. Their advices and guidance immensely helped me to write and complete the thesis.

I would also like to thank Norwegian Petroleum Directorate for providing me the necessary data used in this thesis and University of Tromsø for providing me necessary software.

Finally, I would like to thank my fellow students, friends and family, especially Sofia Zakharova, Daria Martiuk, Andrei Roman, Roberto Maria Ziengs, Andrei Konyaev and Ivan Kolmogorov for motivating and supporting me both during the writing of this thesis and during my whole student life.

Content

1. Introduction

The Barents Sea is a large epicontinental sea which is located above the Arctic Circle north of the shores of Norway and Russia (figure 1.1). The sea is bordered by North-European coasts in the south, islands of Novaya Zemlya in the east, archipelagos of Svalbard and Franz Josef Land in the north and the shelf edge in the west (Faleide et al., 1993; Faleide et al., 1996).

The Barents Sea is also regarded as a hydrocarbon province. In 1970s the exploration of hydrocarbons started, and in 1980s the first wells were drilled (Smelror et al., 2009). Successfully proven fields such as Johan Castberg and Goliat, and discoveries such as Alta, Gotha and Shtokman, showed that the Barents Sea has potential for the development of the petroleum industry. This potential led to the further exploration of the subsurface of the Barents Sea (Smelror et al., 2009; Mattos et al., 2016).

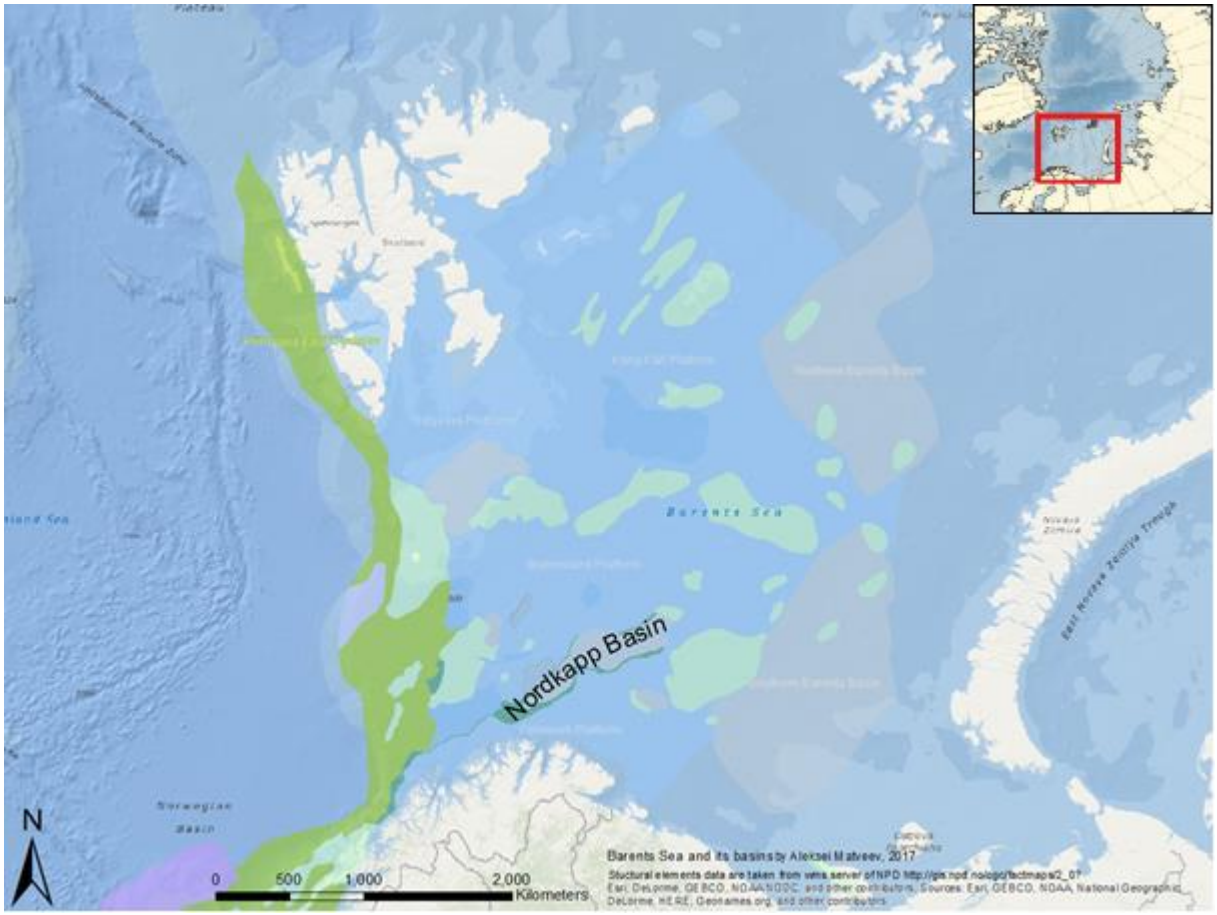

Figure 1.1*: Map showing the Barents Sea, its major structures (in green and grey) and the Nordkapp Basin. Location of the basins are from NDP (2017a), ocean map is from the free map catalogue for Esri ArcGIS.*

The aim of this work is to study the development of the Nordkapp Basin during the Cretaceous period. The basin is influenced by salt diapirism and salt tectonics. Salt structures interrupted Mesozoic layers and created smaller sub-basins between the salt domes (Jensen et al., 1992; Bygge et al., 2002). Series of tectonic events from the Middle Paleozoic to Early Cenozoic developed fault complexes forming fault-related structures (Jensen et al., 1992). Due to massive glacial erosion of the basin in the Pliocene-Pleistocene, the Upper Mesozoic layers are covered with just 100-150 meters of Quaternary sediments in most part of the study area (Bugge et al., 2002).

2. Theoretical framework

This chapter contains definitions and explanations of terminology necessary for further understanding of this work.

2.1 Seismic facies

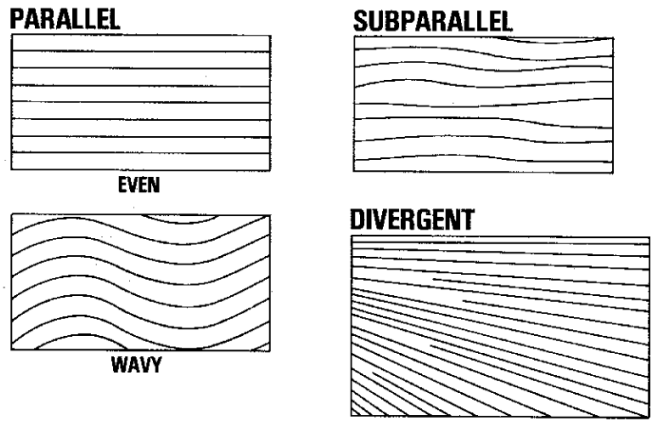

Figure 2.1: *A scheme showing parallel, subparallel and divergent configurations of seismic facies. Modified from Mitchum et al. (1977).*

Seismic facies are three dimensional seismic units which can be distinguished on seismic data. They consist of groups of reflections, parameters of which differ from properties of reflections of adjacent facies units (Mitchum et al., 1977). Seismic facies differ in configuration of their geometry, continuity, amplitude frequency and interval velocity. There are several main geometric configurations of seismic facies, which depend on depositional rate, energy and initial environment (figure 2.1). The first configurations are parallel and subparallel. Parallel configurations are subdivided into even and wavy but the reflectors are still parallel. They are most common in sheet and fill units (Mitchum et al., 1977). Subparallel facies are distinguished from parallel because of other parameters such as amplitude and continuity, and not due to sedimentation rate. Parallel and Subparallel facies imply uniform depositional rates on a stable basin plain or uniformly subsiding shelf (Mitchum et al., 1977)

The other group of seismic facies includes divergent configurated facies (figure 2.1). Such facies occur when lateral changes in deposition rate are present or when angle of inclination of the depositional surface changes during the time (Mitchum et al. 1977).

The third group of reflection configurations are configurations, which occur on prograding slopes. Such configurations are called clinoforms and are subdivided into sigmoid, oblique, complex, shingled, and hummocky (figure 2.2) (Mitchum et al, 1977). Sigmoid pattern (figure 2.2a) is made under conditions with low sediment supply and rapid basin subsidence or sea rise. Depositional angles are often low and the parallel reflectors of the topset slightly change their inclination in a middle part of the feature.

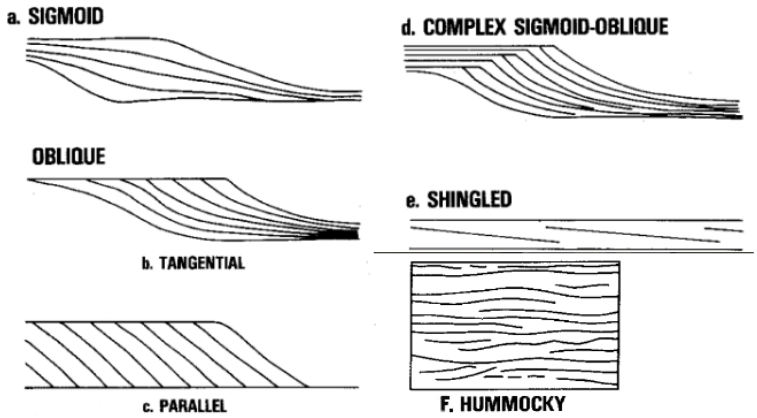

Figure 2.2: *A scheme, showing different types of clinoforms. Figure modified from Mitchum et al. (1997).*

The second pattern, oblique clinoforms (figure 2.2 b, c), are characterized by steep inclination of strata and lack of topset. The angle is significantly higher than angle that is present in sigmoid pattern and may reach more than 10 degrees. The pattern is subdivided into tangential and parallel oblique clinoforms. Both of them imply high sediment supply and constant conditions in the basin during sedimentation, but erosion after deposition (Mitchum et al, 1977).

Another clinoforms, complex sigmoid-oblique, (figure 2.2d) are characterized by rapid change from sigmoid to oblique pattern within the single seismic unit. Such clinoforms are present in the units which were developed under high energy deposition conditions, but changeable sediment supply (Mitchum et al., 1977).

Shingled clinoforms (figure 2.2e) consist of upper and lower parallel surfaces and parallel slightly inclined reflectors between them. These reflectors often have thickness right above the seismic resolution and in some units their inclination is not visible and is only suggested.

Such pattern is present in the units, which were developed in shallow water (Mitchum et al., 1977).

Hummocky clinoforms (figure 2.2f) consist of discontinuous segments of reflectors. Such reflections are subparallel and have non-systematic terminations and breaks. The relief is very low, barely distinguished on seismic data and is at the point of seismic resolution. This pattern is formed in shallow waters of prodelta or in delta itself (Mitchum et al., 1977).

2.2 Salt diapirism

Salt diapirism or halokinesis is an upward salt movement or movement of salt bodies influenced by salt rock buoyancy in denser overlying layers (Trusheim, 1960; Vendeville, 2002). This process was described by Trusheim (1960), who also divided salt movements into three different stages: pillow, diapir and postdiapir (figure 2.3). He assumed that overburden salt is viscous and can move upwards under the certain temperature and pressure caused by overlying rocks according to Rayleigh-Taylor instabilities (Trusheim, 1960). The density of halite, the mineral from which salt rock is mainly formed, is 2.17g/cm^3, which is relatively lower than the average for most of limestones and sandstones with moderate porosity. The pressure conditions needed to force salt rock behave viscous can be created by only a few hundred meters of overlying rocks. Upward movement of viscous salt causes deformation and fracturing of overlying strata. This process is called salt tectonics (Nichols, 2009).

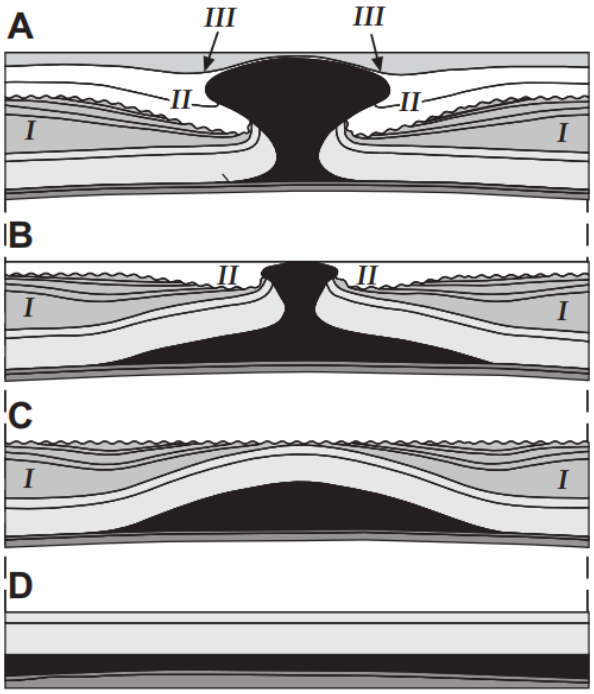

Figure 2.3: *Schematic growth of salt diapirs by Trusheim (1960).* **A**. *Post-diapir (present-day) stage with tertiary synclines (III).* **B.** *Diapir stage with secondary sinks(II).* **C.** *Pillow stage with primary peripheral sinks (I).* **D.** *Initial salt layer before any salt movements. Retrieved from Vendeville, 2002.*

2.3 Faults

Faults are planar discontinuities or breaks of the strata which are related to differential displacement of rock (Peacock et al., 2016). They result in weak zones of layer because of shear failure. On a seismic profile, they appear as a discontinuity of reflection.

There are several types of faults which are caused by different tectonic stress and tectonic regime (figure 2.4). Normal faults are caused by tension of the geological layers which leads to the movement of one block of layers up, while another is moved down. Normal faulting sometimes includes rotation of the blocks involved when the extension is large enough (figure 2.5). Thrust or reverse faults are caused by thrust or compression of rock mass where the block of strata is pushed over another block. This results in strata where young layers are under old layers. Strike-slip faults are caused because of shearing and horizontal movement of blocks (Press et al., 1994, figure 2.4).

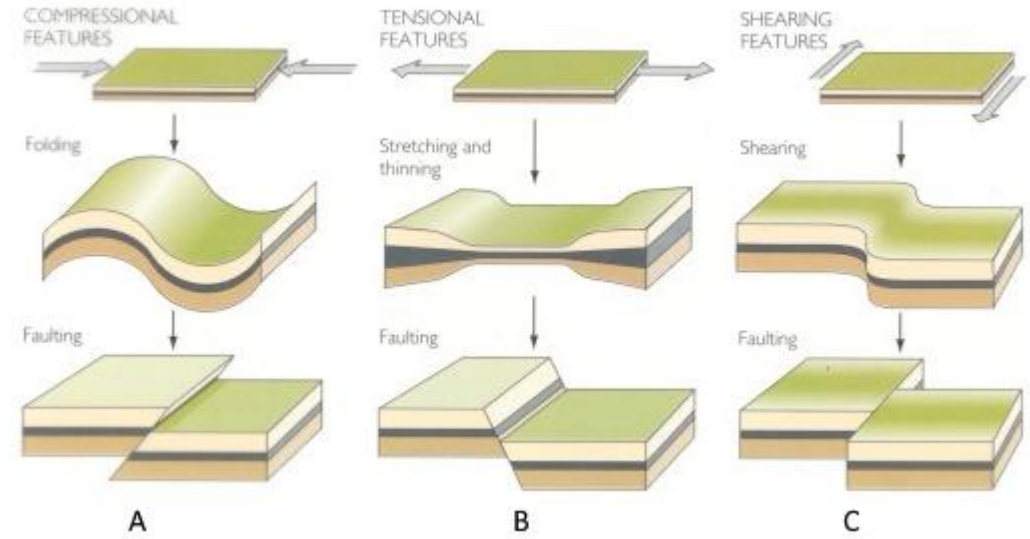

Figure 2.4: *Formation of different fault types.* **A.** *Reversal faults.* **B.** *Normal faults.* **C.** *Strike-slip faults. Modified from Press et al., 1994.*

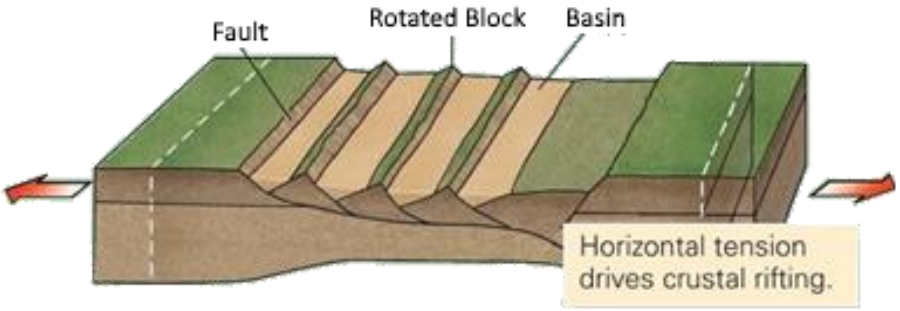

Figure 2.5: *Rotated block faulting. Modified from Marshak, 2012.*

2.4 Petroleum plays, prospects and traps.

According to the definition from Norwegian Petroleum Directorate (NPD) petroleum play is geographically and stratigraphically determined area, where reservoir rock, mature source rock, trap and migration paths are present (NPD, 2017). In other words, petroleum play is a group of petroleum prospects which shear these geological circumstances. Petroleum prospect is an outlined reservoir rock with a trap where resource volume of hydrocarbons is delineated (Stoneley, 1995). Petroleum system is a system which includes the active source rock, migration paths, trap, seal, reservoir rock and all the genetically related discovered oil and gas (Magoon & Beumont, 1999; AAPG, 2017). The main difference between petroleum system and petroleum play is that petroleum system includes only discovered petroleum (Magoon & Beumont, 1999; AAPG, 2017).

A trap is a structure of impermeable layer which prevents fluids from further upward migration from the reservoir. Traps are divided into structural and stratigraphic. Structural traps are traps created by different geological structures such as anticlines and fault complexes (figure 2.6). Stratigraphic traps are caused by sudden difference in permeability of deposited layers (Selley et al., 2014).

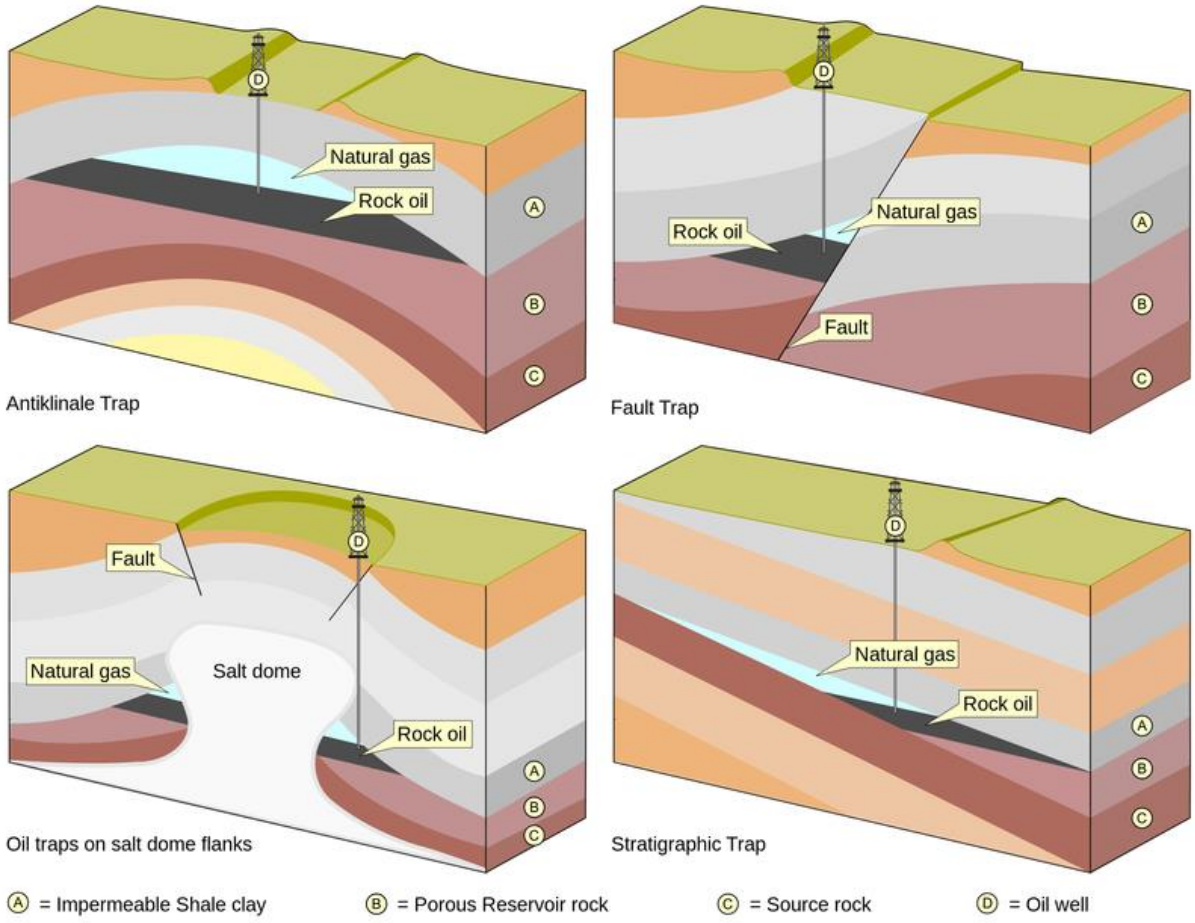

Figure 2.6: *A scheme showing petroleum traps and reservoirs. Retrieved from Hanania et al., 2016.*

Salt tectonics and diapirism can create diapir-associated petroleum prospects by deformation and fracturing of surrounding rocks. Such processes can trigger fluid migrations and form anticlines, synclines and fault structures, which can function as trapping mechanism to keep hydrocarbons stored in reservoir (figure 2.6) (Selley et al., 2014, Hanania et al., 2016).

3. Geological framework

This chapter explains what the Cretaceous Period is and how it was defined. Moreover, the chapter contains geological history of the Barents Sea in general and geological history of the Nordkapp Basin specifically.

3.1 The Cretaceous Period and System

The Cretaceous period is the last geological period of the Mesozoic Era which covers a time interval of 79 million years. It starts from the end of the Jurassic Period ~145 million years ago (Ma ago) and ends at the beginning of the Paleogene Period 66 Ma ago (figure 3.1) (ICS, 2017).

During the Cretaceous Period, the Pangea supercontinent continued to fracture into the modern continents. An opening and development of the warm seas caused a rapid increase of calcareous nanoplankton and foraminifera which produced large chalk deposits. These chalk deposits gave a name to the period (chalk is *creta* in Latin). The period was firstly defined in the Paris Basin by Jean Baptiste Julien d'Omalius d'Halloy in 1822. During the Cretaceous the two major oceanic anoxic events occurred. The first one happened in the Aptian age, and the second one - at the Cenomanian-Turonian boundary. They affected chemical composition of oceans and led to minor extinctions of marine life forms. These events are recorded by sedimentation of black shales (Gradstein et al., 2004).

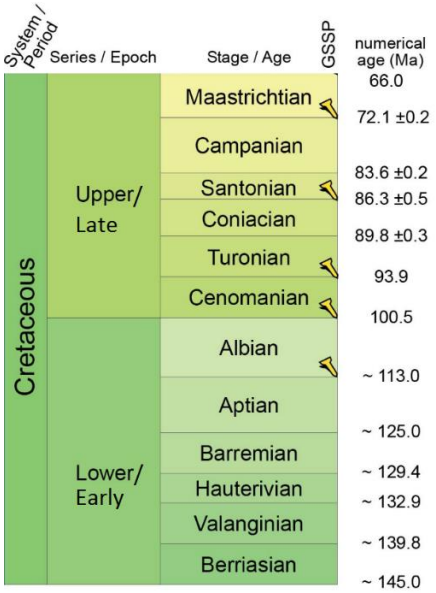

Figure 3.1: *Chronostratigraphic chart of the Cretaceous System and the Cretaceous Period. GSSP - Global Boundary Stratotype Section and Point. Modified form ICS, 2017.*

The period dramatically ended with the Cretaceous-Paleogene extinction 65.5-66 million years ago (Gradstein et al., 2004). This extinction is considered to be caused by impact of an asteroid 10 km in radius which created a 180-km impact crater called Chicxulub in the Yucatán Peninsula (Kring, 1995). The event caused extinction of nearly 75% of species on Earth and changed its history (Jablonski, Chaloner, 1994).

The Cretaceous is divided into twelve stages (figure 3.1). Stratigraphic boundaries between the stages were mainly defined by ammonoids – extinct group of marine molluscs, found in West Europe (France and the Netherlands). The boundary between the Top Cretaceous and Paleocene is visible in most cases on the geological records and represents discontinuity in the fossil fauna. It also has high iridium content (Gradstein et al., 2004). The base of the Cretaceous is not well-defined and is debatable. According to International Commission on Stratigraphy (ICS), the lowest stage is set because of limestone with ammonoid fossil deposits found near the village Berrias in France (Gradstein et al., 2004).

3.2 Regional setting

The Barents Sea is located north of the coasts of northernmost Europe. As it was previously described in introduction, it is surrounded by archipelagos of Svalbard, Frantz Josef Land and Novaya Zemlya and north costs of Norway and Russia (figure 1.1). It covers area of 1.3 million square kilometers and has an average water depth of near 300 meters (Dore, 1995).

The sea covers multiple sedimentary basins (Jensen et. al, 1992) and is located on a continental margin, which was developed when the Atlantic and Arctic oceans opened in response to the Paleocene break-up between the Scandinavian Peninsula and Greenland (Dengo et al., 1992).

3.2.1 Geological evolution of the Barents Sea

The earliest recorded tectonic event in the Barents Sea is Caledonian Orogeny which is related to collision between continents of Baltica and Laurentia and formation of supercontinent Euramerica. In Scandinavia it happened 425-400 million years ago in the Late Silurian-Early Devonian (Dengo et. al, 1992, Jones et. al. 2003). The event led to compression and deformation of the crystalline basement (Gernigon et al., 2011, Mattos et al., 2016) and

formation of grabens in the western Barents Region (Gernigon et al., 2011, Faleide, 1996) (figure 3.2a). The tectonic events, which followed the Caledonian Orogeny, started with initialization of regional rifting between Norway and Greenland in Late Devonian to Early Carboniferous (Dengo et al., 1992, Gernigon et al., 2011). This led to the formation of some elongated basins with northeast trending. One of them is the Nordkapp Basin (Jensen et al., 1992, Gernigon et al., 2011) (figure 3.2b).

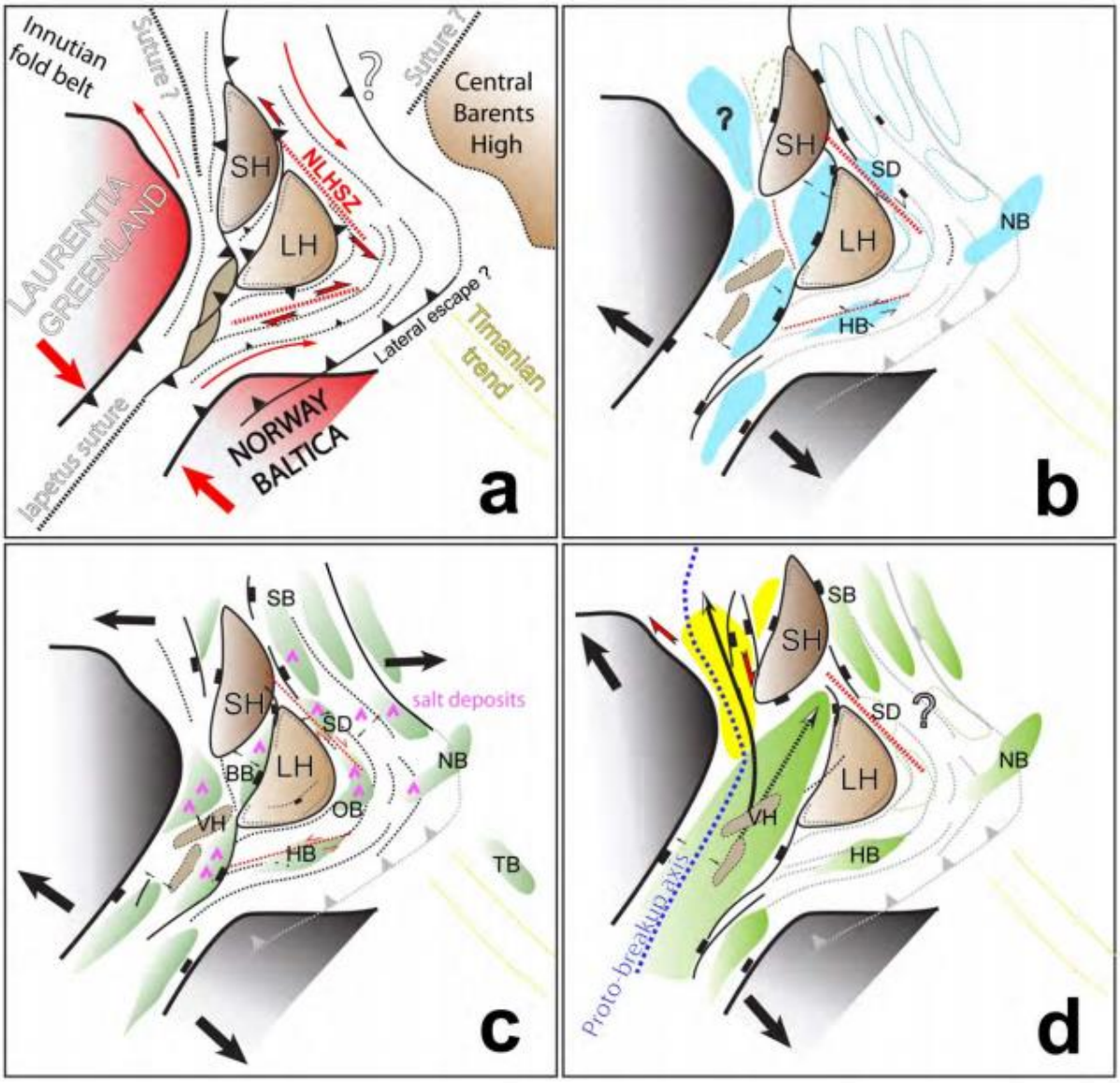

Figure 3.2: *Conceptual models of the geodynamical evolution of the southwestern Barents Sea from Late Devonian to Late Mesozoic time.* **a)** *Late Devonian post-orogenic collapse of the Caledonides between Laurentia and Baltica.* **b)** *Carboniferous reactivation of the main features and shear zones and graben development.* **c)** *Early to Mid-Mesozoic rifting episodes, graben formation and salt tectonics.* **d)** *Late Mesozoic crustal thinning and westward migration of the deformation. BB – Bjørnøya Basin, HB – Hammerfest basin, LH – Loppa High, NB – Nordkapp Basin, OB – Ottar Basin, SB – Sørkapp Basin,*

SD – Svalis Dome, SH – Stappen High, TB – Tiddlybanken Basin, VH – Vestlemøy High, Modified from Gernigon et al., 2011.

Rifting stopped for a while in the Late Permian (Mattos et al., 2016). This created space and conditions for evaporite deposition in this area in the Late Carboniferous to Asselian age of Permian (Jensen et al., 1992). Moreover, this period is marked with the beginning of thermal subsidence in the Barents Sea area (Dengo et al., 1992). The tectonic plate, where the today's Barents Sea was positioned, continued to move in north direction during the Permian and passed through a climatic belt with semi-arid conditions (Mattos et al., 2016). Warm and hot climate caused development of reefs and deposition of carbonates (limestones). This led to development of a carbonate sequence (post-rift carbonate platform) of regional extent (figure 3.3) (Jensen et al., 1992, Mattos et al., 2016, NPD, 2014a).

Form the Late Permian subsidence rates of the Barents Sea increased as a response to Hercyanian orogeny in the east and formation of Ural Mountain Chain (Faleide et al., 1984, Mattos et al., 2016). This, together with the further north movement of a plate, resulted in a more humid climate, which led to change in deposition from carbonates to clastic and organoclastic sediments derived from Uralian Orogen (Jensen et. al., 1992; Smelror et al., 1993). Series of changes in the sea level caused deposition of strata, which are clearly seen on the Late Permian - Triassic sequence (NPD, 2014, Jensen et al., 1992).

Passive subsidence of the area continued during the Triassic period (Mattos et al., 2016; Smelror et al., 2009; Faleide et al., 1992). This created anoxic conditions on the sea bottom which were present up to the Anisian – Ladinian Age of the Triassic Period, where in the Middle Triassic organic-rich mudstone was deposited and accumulated (Smelror et al., 2009; Mattos et al., 2016). This led to formation of source rock in areas of the greater Barents Sea (Steinkobbe Formation, Klappmyss Formation) (figure 3.3) (Bjoroy et al, 2009; Smelror et al., 2009; NPD, 2014). Such variations in sediment deposition together with active faulting increased gravitational instability in the subsurface. This triggered an upward movement of Permian salts which started in the Middle to Late Triassic (Jensen et al., 1992; Smelror et al., 2009) (figure 3.2c). In the end of the Triassic Period a tectonic event caused further extension of the Barents Sea and formation of coastal plain (Faleide et al., 1984; Smelror et al., 2009).

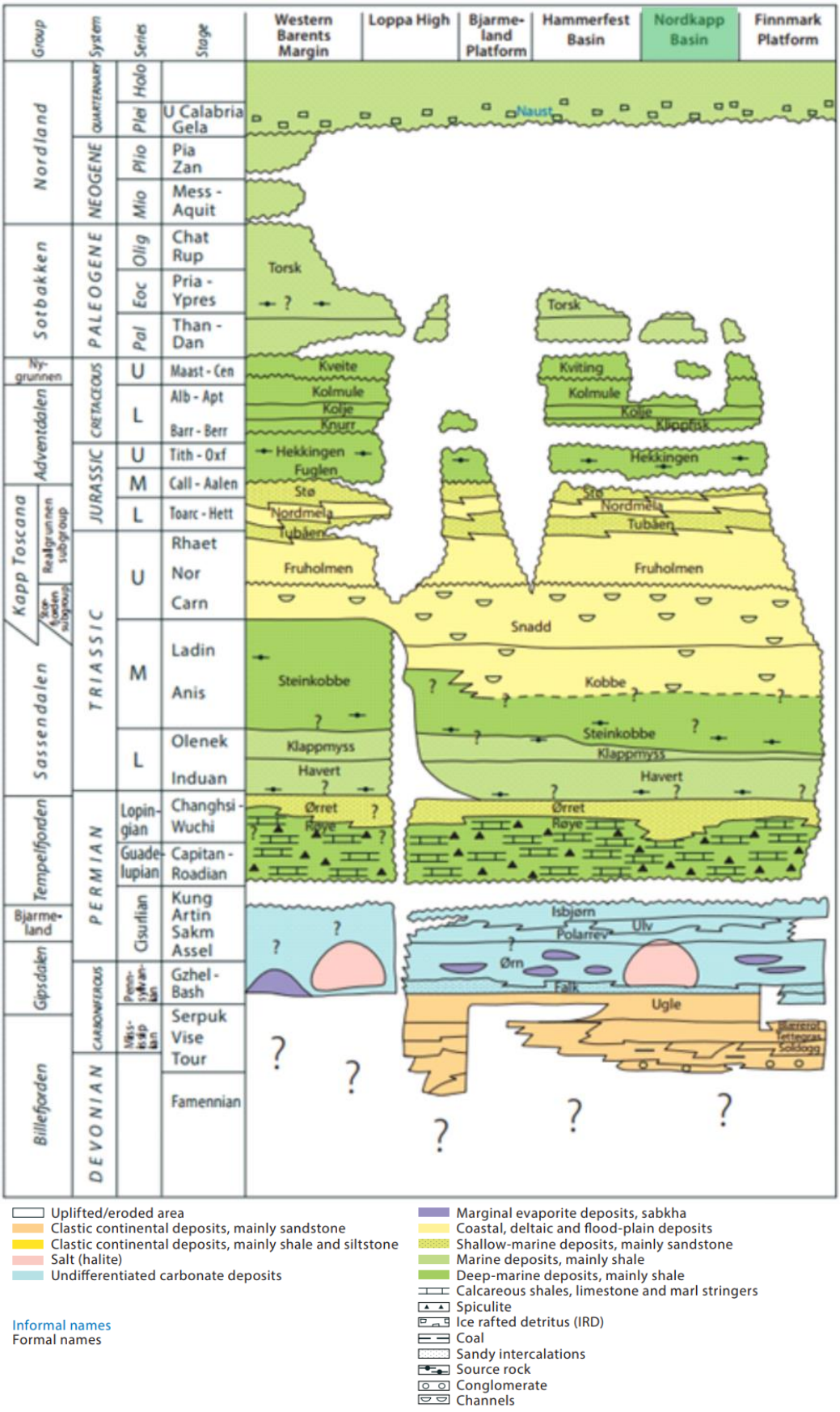

Figure 3.3: *Lithostratigraphic chart of the Norwegian part of the Barents Sea. Study area is highlighted with green. Modified from NPD, 2014a.*

During the Jurassic period, several tectonic events took place in the area between Greenland and Norway (Faleide et al., 1984, Faleide et al., 1993, Dengo et al., 1992). The major phases were in Hettangian-Pliensbachian, Aalenian-Bajocian and Kimmeridgian ages (Faleide et al., 1984, Mattos et al., 2016). The second phase affected the North Atlantic and opened a large marine gateway from the southwest to the areas of the greater Barents Sea. This led to transport of mature and well-sorted sandstones from the main ocean and their further deposition in the Stø Formation (Ramberg et al., 2008; Mattos et al., 2016).

The third phase influenced the sea the most and led to rapid subsidence of areas between Greenland and Norway (Faleide et al., 1984). The second and the third phases in the Middle to Late Jurassic developed strike-slip fault systems which were initially formed in the Early Carboniferous (Mattos et al., 2016, Faleide et al., 1984, Dengo et al., 1992). This led to formation of large basins surrounded by salt diapirs and structural highs (Smelror et al., 2009; Mattos et al., 2016). In the Late Jurassic (Tithonian) a sea level reached its maximum. This led to deposition of mainly clay sediments in open marine environments over the most part of the Barents Sea during this time (Krill member of the Hekkingen Formation on figure 3.3). Since then, the regression of the region started (Smelror et al., 2009).

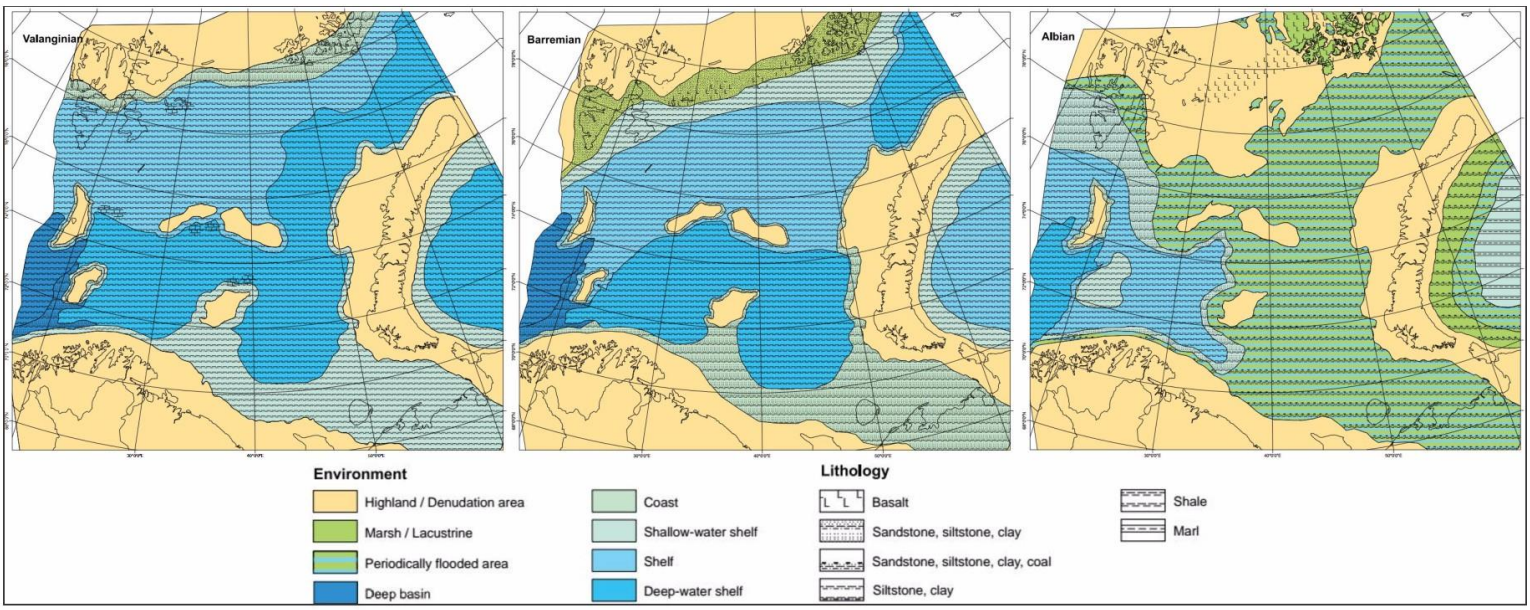

Figure 3.4: *Environments of the Barents Sea during the Early Cretaceous. Modified from Smelror et al., 2009.*

During the Cretaceous the northern parts of the Barents Sea were uplifted as a response to opening of the Amerasian basin in the Arctic Ocean (Figure 3.4). There are evidences of small repeated glaciations in the North Barents Sea during this time, but overall climate remained warm and humid. The climate, together with continued uplift, reduced marine sedimentation and increased sediment supply from the north (Smelror et al., 2009).

During the Barremian-Albian age (figure 3.4), the large deltas were developed from the north to the south, increasing terrigenous sediment supply (Smelror et al., 2009). This led to deposition of the thick sequences of the Lower Cretaceous sediments (Smelror et al., 2009). The uplift of the North Barents Region was accomplished by volcanic activity (Smelror et al., 2009; Faleide et al., 1984). Continued regional uplift of the Svalbard Platform and rifting in the North Atlantic increased development of faults in the west parts of the Barents Sea during the Late Cretaceous (figure 3.2d) (Faleide et al., 1984; Mattos et al., 2016).

The Paleogene started with strike-slip deformation in area between Greenland and Norway (Breivik et al., 1998; Mattos et al., 2016). During the Paleocene – Early Eocene, tectonic rifting and continental break up along the North Atlantic Ridge opened and developed Norwegian Sea (Faleide et al., 1996). These events boosted movement of salts and increased the faulting in the western Barents Sea. Northern and eastern parts of the Barents Sea were uplifted, however subsidence continued in the westernmost basins during the Eocene and led to increase in deposition there due to sediment supply from the uplifted areas (Smelror et al., 2009). This led to transport of sediments from the eastern parts to the western basins and development of the submarine fans in the area (Smelror et al., 2009; Faleide et al., 1996, Mattos et al, 2016). From the Middle Miocene, the whole Barents Sea began to uplift, which led to further development of submarine fans (Faleide et al., 1996; Smelror et al., 2009). During the Pliocene-Pleistocene, glacial erosion boosted the uplift of the Barents Sea especially in its north-east parts. This led to erosion of nearly 1200 meters Cenozoic and parts of Upper Mesozoic sediments and formation of the Upper Regional Unconformity (Dengo et al., 1992; Faleide et al., 1996; Smelror et al., 2009).

3.3 Study area: the Nordkapp Basin

The Nordkapp Basin is located in the eastern part of the western Barents Sea (figure 1.1, figure 3.5). The basin has an overall southwest-northeast direction and is believed to be a rift basin

controlled by fault complexes of Nysleppen in northwest, Polstjerna in north, Måsøy in south and Thor Iversen in east (figure 3.5) (Halland et al., 2014; Mattingsdal et al., 2015). Måsøy and Thor Iversen fault complexes separate the basin from the Finnmark Platform, while Nysleppen and Polstjerna fault complexes separate it from the Bjarmeland Platform. The northernmost part of the Nordkapp Basin is bounded by Veslekari Dome, which is a huge salt structure 50 kilometers long and 25 kilometers wide (Mattingsdal et al., 2015). The Nordkapp basin is strongly influenced by salt tectonics, originating from the halite deposited during the Late Carboniferous – Early Permian (section 3.2.1) (Dengo et al., 1992). The basin is 350 km long and has maximum width up to 80 km (Jensen et al., 1992). The basin can be divided into two parts (southwest and northeast), which are separated by a tiny "bottleneck" 30 km wide (figure 3.5) (Jensen et al., 1992).

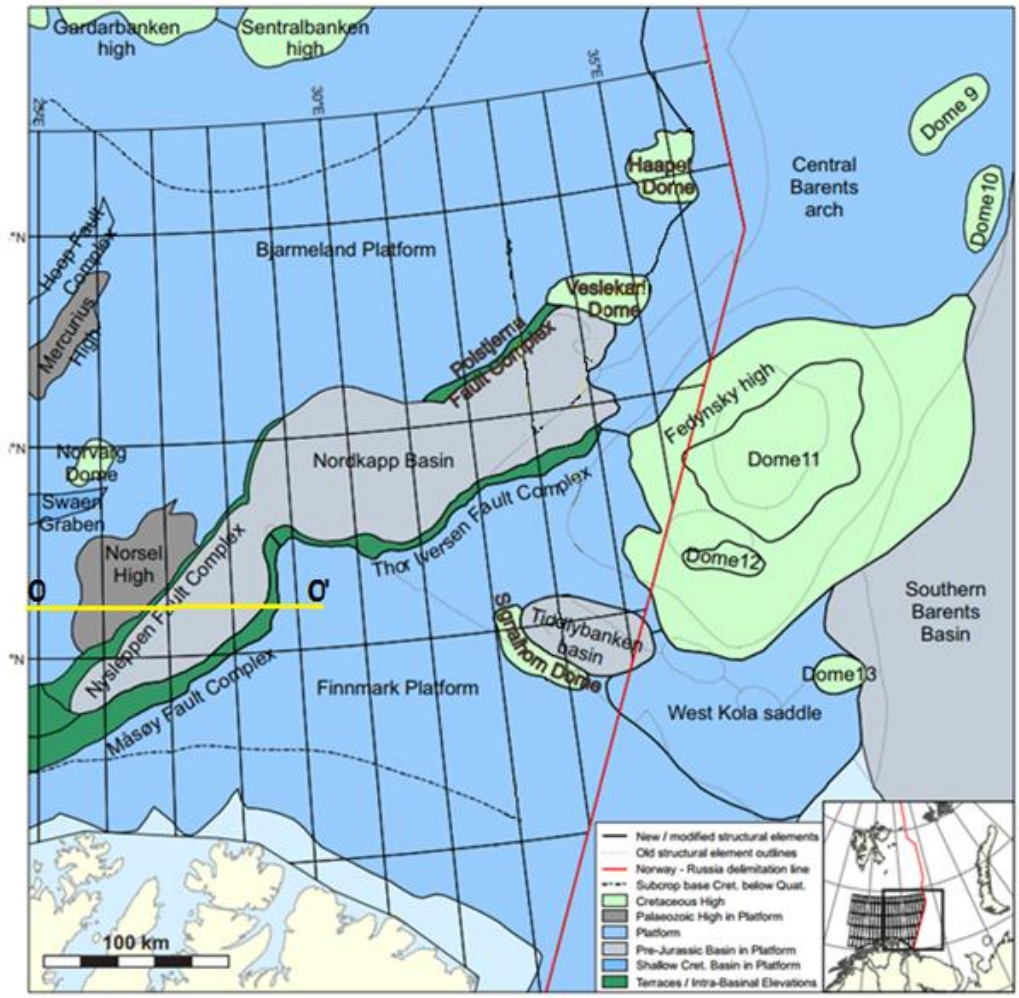

Figure 3.5: *The Nordkapp basin and nearby structures. Modified from Mattingsdal et al., 2015.*

The south part of the Nordkapp Basin and fault complexes surrounding it were created during rifting in the Early Carboniferous, which was described above (section 3.2.1) (Jensen et al., 1992).

Halokinesis in the basin started in the Early Mesozoic and was triggered by weight of deposited sediments and active faulting (Dengo et al., 1992; Jensen et al., 1992; Halland et al., 2014). The model of salt tectonics deviates from the Trusheim (1960) model because of lack of primary rim synclines (Jensen et al., 1992). This led to conditions where petroleum traps associated with formation of salt pillows are not expected to be found. However, traps related to secondary rim synclines and flanks of the diapirs are present (Jensen et al., 1992). Salt structures uplifted overlying sediments and led to formation of smaller sub-basins between the salt domes (Jensen et al., 1992). The Uralian orogeny and formation of huge river systems led to deposition of clastic sediments (mainly porous sandstones) during the Middle Triassic – Middle Jurassic (Smelror et al., 2009; NPD, 2014). The series of rifting events from the Early to the Late Jurassic, described above (section 3.2.1), developed faults which surrounded the basin that time (Faleide et al., 1993; Breivik et al., 1998).

The thick sequences of Lower Cretaceous sediments are present in the basin (Figure 3.6). Their deposition was influenced by the processes such as regional uplift and deltas development during the Cretaceous Period (section 3.2.1) (Smelror et al., 2009).

Due to glacial erosion (section 3.2.1), the topmost parts of the Mesozoic strata, which are present in most parts of the basin, are Lower Cretaceous layers and they are covered with only 100 meters of Quaternary sediments (Smelror et al., 2009). However, in a few places the Upper Cretaceous and even Paleogene strata are present (figure 3.6).

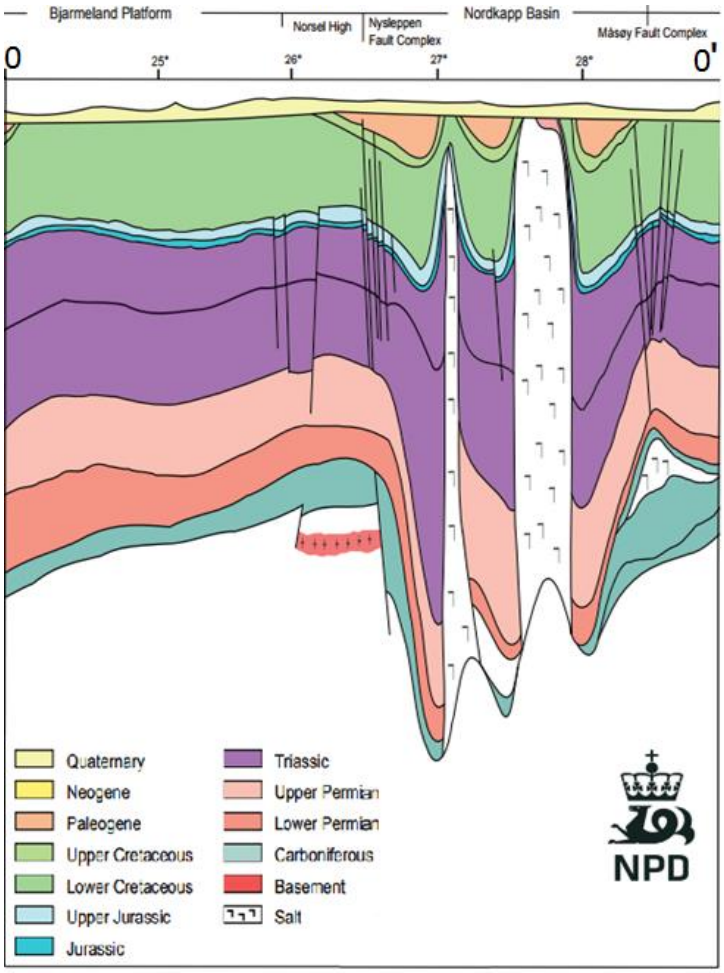

Figure 3.6: *Stratighraphy of the Nordkapp Basin and nearby structures. Position of the 00' profile is shown on figure 3.5. Modified from NPD 2014b.*

4. Data

4.1 Data overview

During this work, 2D seismic data covering the Nordkapp Basin is used. Data is provided by NPD (table 4.1) (figure 4.1). The interpretation of the data is made by Schlumberger Petrel 2016 software. Mapping of the data is made by ESRI ArcMap and CorelDraw. 3D seismic surfaces are made by interpretation of seismic horizons on 2D seismic profiles and stacking them into one surface.

In addition to 2D seismic data, well data given by NPD is used to correlate seismic data with lithostratigraphy. The applied wells are 7228/2-1S, 7226/11-1, 7227/10-1, 7228/7-1A and 7229/11-1. The wells are located in the Nordkapp Basin and on Finnmark and Bjarmeland platforms close to the basin (figure 4.2)

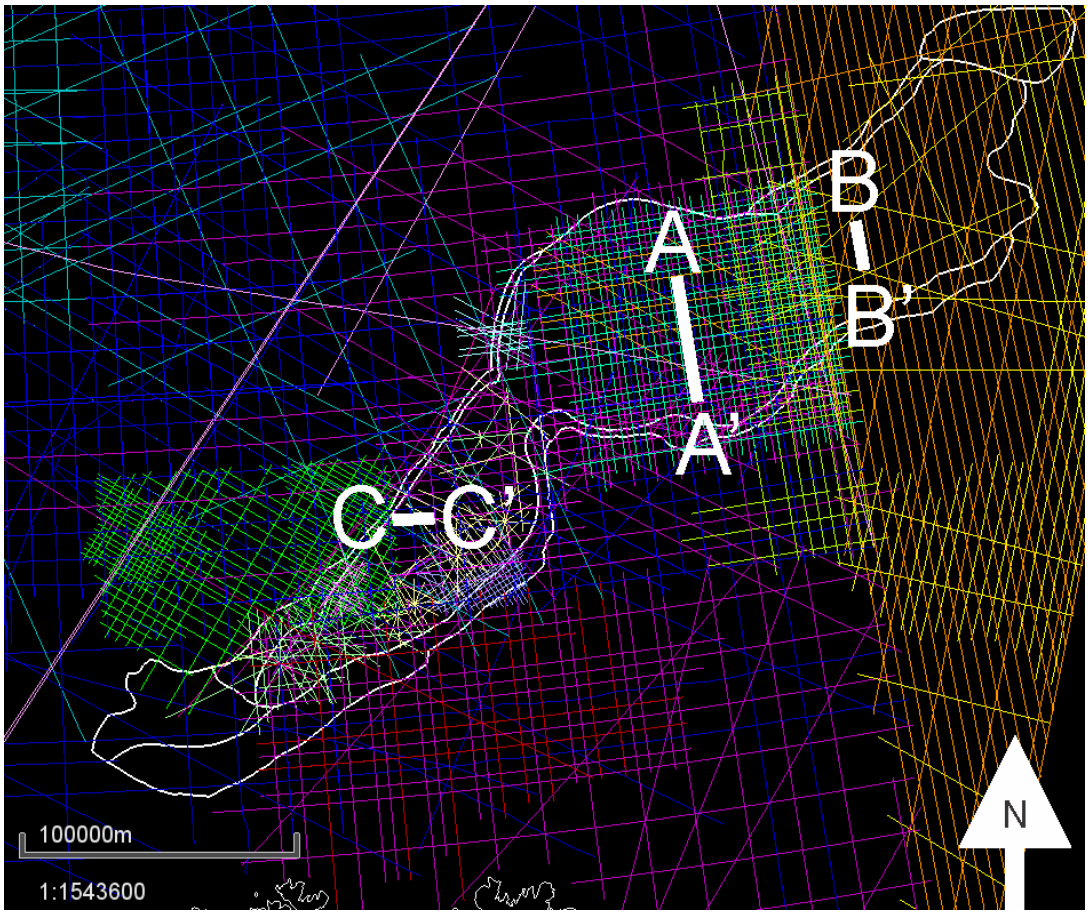

Figure 4.1: *Map of the Nordkapp Basin and adjacent fault complexes showing seismic datasets used in this work and seismic profiles AA', BB' and CC'.*

Well 7228/7-1A is a wildcat well drilled in the Nordkapp basin in 2001 with a main purpose to test the hydrocarbon potential of Triassic sandstones of the Snadd Formation. It was drilled as a sidetrack of well 7228/7-1S and reached depth of 2880 meters. The main operator was Den Norske Stats Oljeselskap AS (Statoil). Oil and gas presence was proven in the Lower Carnian sandstones of the Snadd Formation and the Klappmys Formation with gas-oil contact at 2086 meters depth. The well was abandoned as an oil and gas discovery (NPD, 2017c).

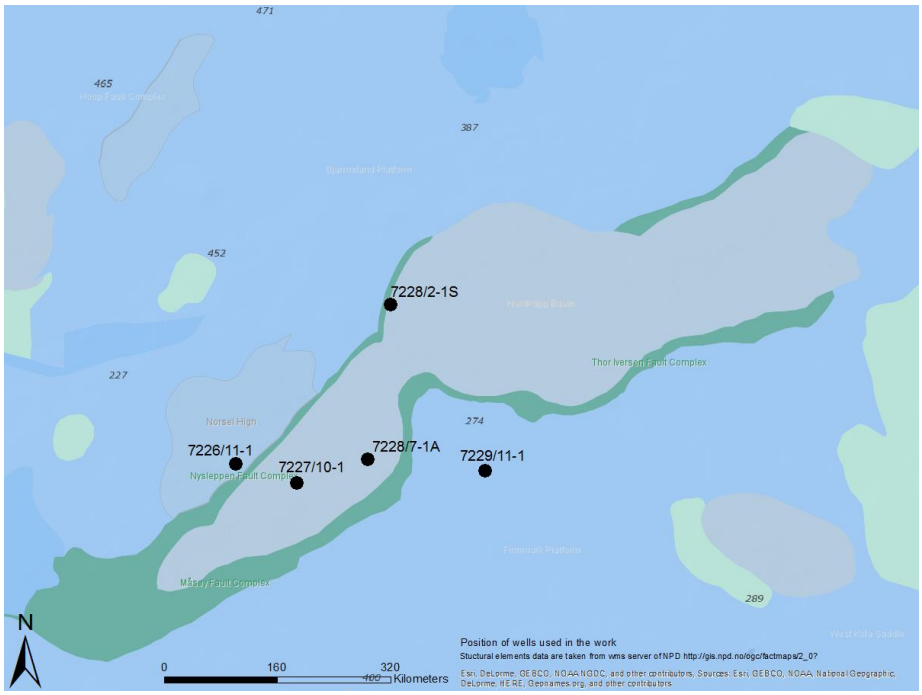

Figure 4.2: *Map of the Nordkapp Basin and nearby structures showing position of wells used in this work. Structural elements and well locations are taken from NPD 2017a.*

Well 7227/10-1 was drilled in in the Nordkapp Basin in 2014 by Statoil Petroleum AS as a wildcat well with the main objective to prove commercial oil volumes of Carnian sandstones in the Snadd Formation. The secondary tasks were to test hydrocarbon potential and presence of the source rock in the Early-Middle Triassic layers. There were not found hydrocarbons in reservoirs penetrated, only trace oil. However, a 2.5-meter source rock at the base of the Snadd Formation (2780 meter) was observed. Well was abandoned as a dry well with the bottom depth of 3135 meters (NPD, 2017c).

Well 7226/11-1 was drilled in 1987-1988 by Statoil as a wildcat well. It is located on the Bjarmeland Platform close to Nordkapp Basin with a bottom depth of 5200 meters. The main

purpose was to test Jurassic-Triassic sandstones and Permian carbonates. Gas presence was found at 2913 meter in Havert Formation (Induan age). The well reached basement at 5137-meter depth and was abandoned as a gas discovery (NPD, 2017c).

Well 7228/2-1S was drilled by Mobil Development Norway AS as a wildcat well in 1989 on the western margin of the Nordkapp Basin and reached 4000-meter depth. The main goal was to test Middle Triassic sandstones. There were found only traces of residual oil, however there were found source rock sequences in Hekkingen, Snadd and Kobbe Formations. The well was abandoned as a dry well (NPD, 2017c).

A wildcat well 7229/11-1 was drilled in 1993 by AS Norske Shell with the main objective to test Permian-Carboniferous prospect. The well is located on the Finnmark Platform south-east of the Nordkapp Basin. The well reached 4627 meters, but did not encounter any hydrocarbons and was abandoned as a dry well (NPD, 2017c).

4.2 Seismic resolution

One of the methods used to study sea subsurface is marine seismic exploration. The exploration is based on production of artificial sound waves and recording the reflected sound (basically echo). While going through the subsurface acoustic wave reflects from underlying layers or structures with different acoustic impedance (AI) (equation 4.1).

$$Z = \rho \cdot v$$

Equation 4.1: *Relationship between acoustic impedance (Z), density of a layer (ρ) and velocity of a seismic sound in medium (v).*

The higher is the difference of acoustic impedance of attached mediums, the stronger is the reflected signal (equation 4.2). Such continuous contrasts in reflection on a seismic wavelet are called reflectors.

$$R = \frac{Z_2 - Z_1}{Z_2 + Z_1} = \frac{\rho_2 \cdot v_2 - \rho_1 \cdot v_1}{\rho_2 \cdot v_2 + \rho_1 \cdot v_1}$$

Equation 4.2: *Reflection coefficient (R) at normal incidence. Where Z_1, ρ_1, v_1 are acoustic impedance, density and velocity of the upper layer and Z_2, ρ_2, v_2 and are acoustic impedance, density and velocity of the lower layer.*

On a seismic profile depth is usually shown as two-way travel time (TWT) – time, needed for a seismic signal to travel from a shot point to a reflector and back to a receiver. A measure, which describes how close such layers or objects can be to each other and can be still distinguishable on the recorded data, is called resolution (Sheriff, 2006). In seismic it is divided into vertical and horizontal resolution.

Vertical resolution is defined by one quarter of wavelength (equation 4.3). It shows the minimum thickness required for sediment to produce reflection visible on seismic wavelet (Yilmaz, 2001; SEG, 2017).

$$\text{Vertical resolution} = \frac{\lambda}{4} = \frac{v}{4f}$$

Equation 4.3: *Vertical resolution. Where λ is a wavelength, v – velocity and f - frequency.*

Horizontal resolution (equation 4.4) depends on the size of the Fresnel zone, which is the horizontal part of a reflector covered by a seismic wave front (Andreassen, 2009).

$$\text{Horizontal resolution} = 2 \cdot R_f = v \cdot \sqrt{\frac{t}{f}}$$

Equation 4.4: *Horizontal resolution. Where v is velocity, t is two-way travel time, f is the dominant frequency and R_f – radius of the Fresnel zone.*

The general trend is that seismic velocity of sound wave increases with depth, while its amplitude and frequency decrease due to loss and geometrical spread of energy. This cause resolution to decrease with depth (Yilmaz, 2001; Andreassen, 2009).

Horizontal resolution can be improved by migration and reduction of the Fresnel Zone. In two-dimensional seismic the migration along the seismic line shrinks the Fresnel zone into ellipsoid with width of one quarter of the wavelength (Yilmaz, 2001; SEG, 2017).

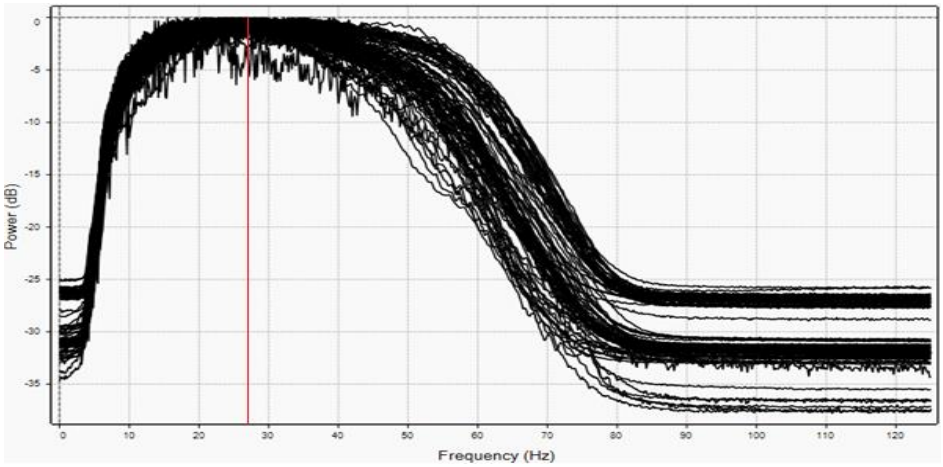

Figure 4.3: *Frequency spectrum for seismic profiles taken during survey BARE02.*

Survey BARE02 was finished in December 2002 (TGS, 2017). Frequency analysis of survey BARE02 (figure 4.3) shows that the average dominant frequency for all of the profiles from survey is 27 Hz. Taking into account the average sound velocity in this area of 2200 m/s (Andreassen, 2009), it is possible to estimate an average vertical resolution of the data using equation 4.3. $\frac{2200m/s}{4*27Hz} \approx$ 20 meters.

For the rest of the datasets the same procedures as for the dataset BARE02 are made (table 4.1). Analysis of quality of the given seismic data gives variation in vertical resolution from 12 to 50 meters.

For most of the datasets from 80s-90s the average dominant frequency is generally lower than for the surveys made during the current century and do not exceed median frequency of 20 Hz (for example for the dataset SG8837 it is only 11Hz (table 4.1) (figure 4.4)). There is also a logical tendency to increase of the quality of the datasets by time (figure 4.5). Moreover, variance from the average resolution decreases through the time, which affects both minimum and maximum vertical resolution.

However, it is easy to notice that most of the surveys available were made during 80s (figure 4.6), which affects the total quality and increases difficulties with interpretation. The average vertical resolution for the all datasets is calculated as 31 meters (table 4.1), which is enough for the interpretation of the main and thick Cretaceous sequences, but is too low for the visualization of relatively narrow formations such as Klippfisk and Knurr (see section 5.2). Moreover, due to poor quality of some of the old datasets it is difficult and in some cases

impossible to interpret even the strong reflectors (for example Base Cretaceous Unconformity). This is especially critical in such diapiric environment which is present in the Nordkapp Basin (see section 4.3).

Survey	Year	Shot for	Shot by	Length [m]	Dominant frequency [Hz]	Vertical resolution [m]
NPD-BJRE-84	1984	NPD			20	28
NPD-FI-84	1984	NPD			23	24
NPD-NOLO-85	1985	NPD			20	28
IKU-86-NOK	1986	IKU	GECO	2 153 787	40	14
NPD-FiØ1-86	1986	NPD			24	23
NPD-FIØ2-86	1986	NPD			11	50
NPD-NOK1-86	1986	NPD			11	50
SBL-86	1986	WESTGEC	GSI	4 449 672	23	24
GNB-87	1987	WESTGEC	GECO	5 246 485	16	34
IKU-87-NK	1987	IKU	MASTER	579 133	47	12
MN87-4	1987	MOBIL	MOBIL	2 119 687	19	29
SG8837	1988	SAGA	GECO	1 179 404	11	50
SH8810	1988	SHELL	DIGICON	585 273	25	22
ST8825	1988	STATOIL	WESTERN	554 611	11	50
MN89-8	1989	MOBIL	MOBIL	76 120	20	28
MN9004	1990	MOBIL	WESTERN	270 293	13	42
NBGS-90	1990	STATOIL	WESTERN	1 220 431	25	22
ST9007	1990	STATOIL	WESTERN	228 284	14	39
NPTN92	1992	GEOTEAM	GEOTEAM	735 118	16	34
ST9411	1994	STATOIL	GECO	669 772	14	39
MN9902	1999	MOBIL	MOBIL	1 177 724	23	24
IS-CNB-01	2001	INSEIS	CGG	3 619 721	14	39
BARE02	2002	FUGRO	FUGRO	20 177 071	27	20
BARE05	2005	FUGRO	FUGRO	25 482 363	20	28
IS-CNB-06	2006	INSEIS	INSEIS	2 574 617	20	28
NBR06	2006	FUGRO	FUGRO	4 796 009	27	20
NPD-BA-11	2011	NPD	DISKOS	11 748 000	14	39
NPD1201	2012	NPD	DISKOS	6 881 000	18	31
Total average vertical resolution [m]:						31

Table 4.1: *Overview over surveys used in this work. Data about length, customer and operator is from NPD (2017a).*

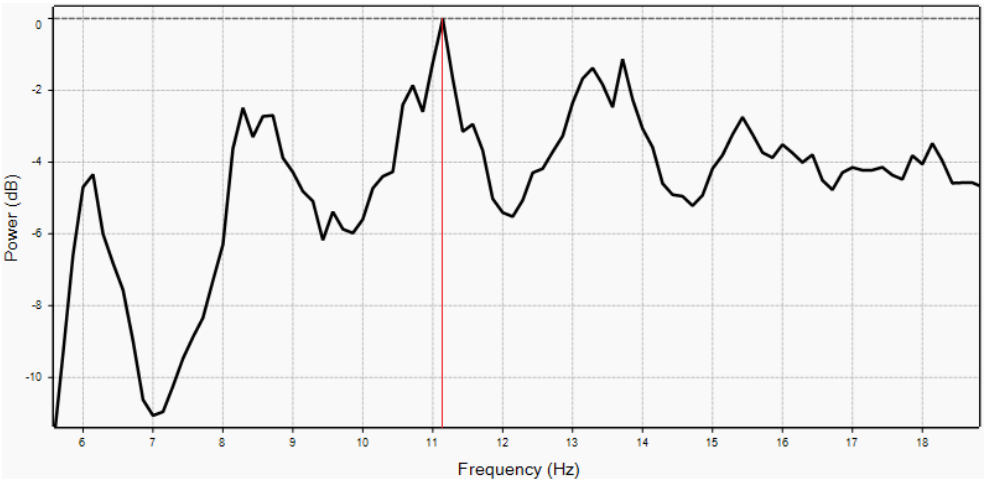

Figure 4.4: *Zoomed frequency spectrum for the seismic profile SG8837-122 from the dataset SG8837 with clearly seen dominant frequency.*

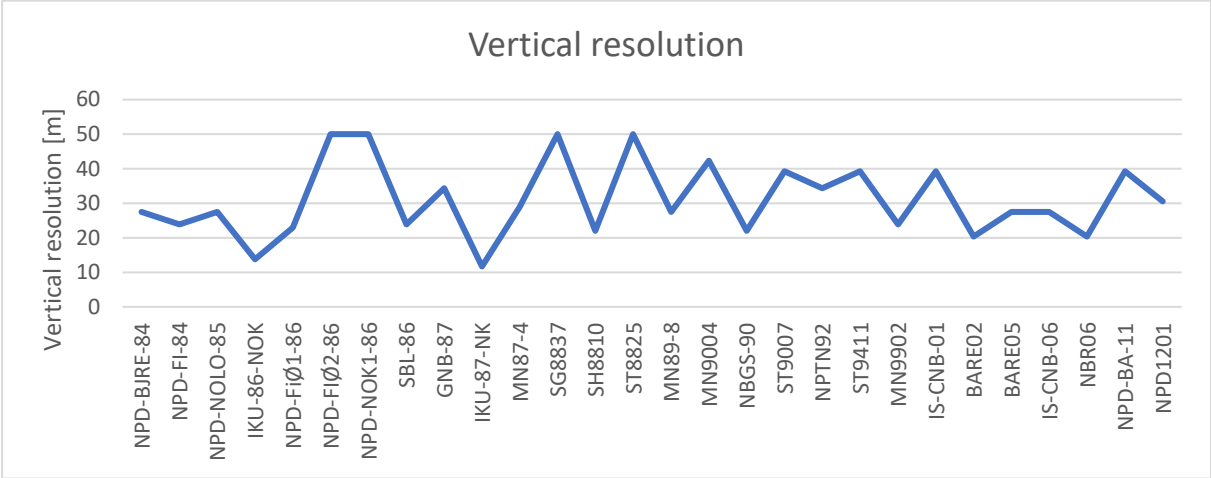

Figure 4.5: *Graph showing vertical resolution among the available datasets. Graph is based on table 4.1*

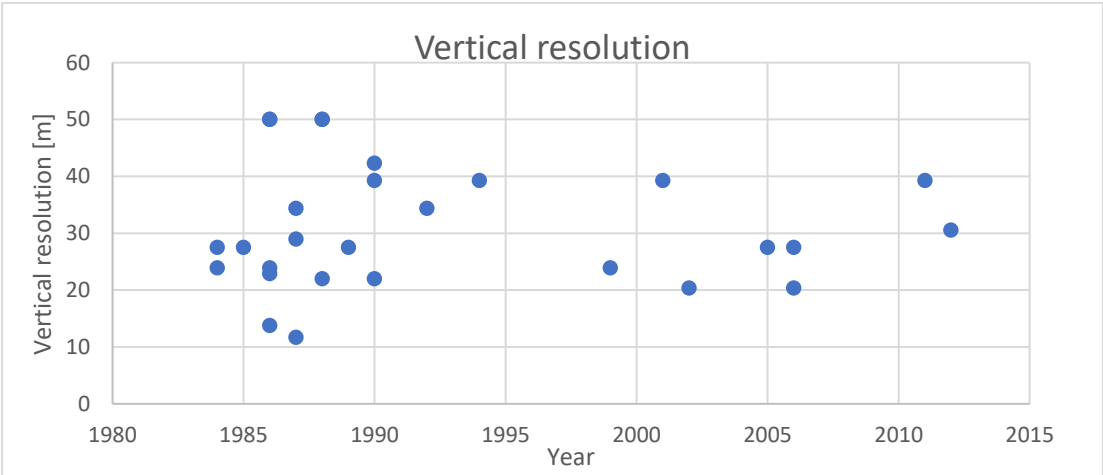

Figure 4.6: *Dotted plot showing average vertical resolution compared to the year of survey. Graph is based on table 4.1*

4.3 Methods and interpretation of diapirs

The interpretation of salt diapirs is based on the outlining of the distorted sound they reflect. The diapirs consist of non-permeable non-porous salt rock, which can be easily seen on seismic surveys, due to higher seismic velocity of seismic P-wave in salt (4700-5500m/s) (Bourbié, 1987). In seismic data, the main body of a diapir is often seen as an area full of noise and discontinuous reflections. The diapir body is mostly homogenous, so strong reflections occur on a top border of the diapir (figure 4.8, figure 5.2).

Mapping of salt diapirs is complicated by the noise and distortions they produce on seismic. For example, the salt structures can serve as lenses for reflected waves (figure 4.7a). This contorts a reflector on the result image and leads to mistakes during interpretation. Another type of errors is a double bounce of the primary ray, where the wave reflects one more time away from the diapir (figure 4.7b). This produces confusing features on the seismic wavelet and makes interpretation more difficult. Moreover, salt diapirs can simply lead to diffraction of seismic waves on their sides both inside and outside due to high seismic impedance difference of salt and nearby sediments (figure 4.7, figure 4.7d). This produces noise and draws weird structures on the seismic profile and can lead to misinterpretation. Diffracted waves can bounce multiple times inside the diapir and increase the amount of noise on seismic wavelet (figure 4.7d) (Jones et al., 2014).

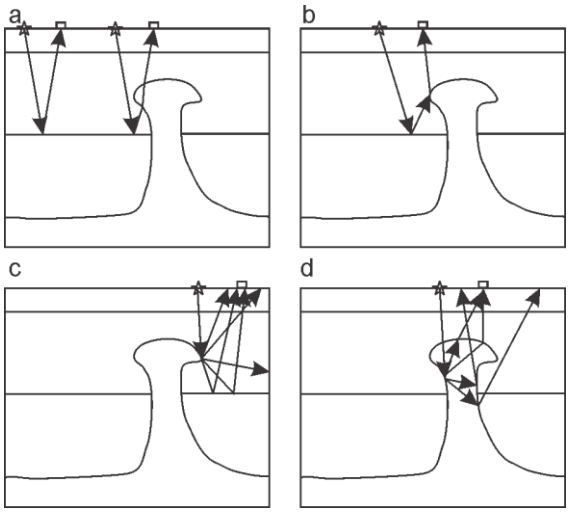

Figure 4.7: *Sketches showing noise and distortions produced by salt diapirs.* **a)** *Raypaths away from and near to the salt diapir.* ***b)*** *Double bounce of the primary ray* **c)** *Diffraction outside the diapir* **d)** *Diffraction inside the diapir and bounce of reflection. Shot point is shown as a star, receiver as a rectangle. Figures are based on Jones at al., 2014.*

In order to map the seismic horizons in the sub basins between salt domes jump correlation method is used. The method includes correlation of similar looking reflectors which have nearly the same depth, reflection amplitude, thickness and are located on the opposite sides of a salt dome (figure 4.8).

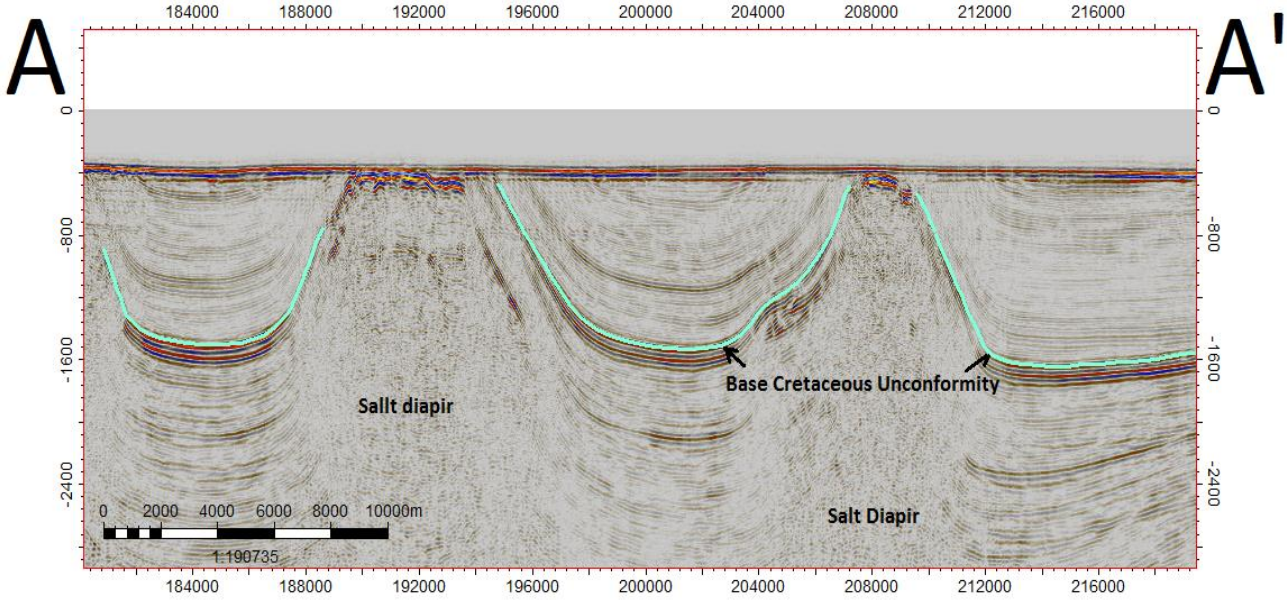

Figure 4.8: *Seismic profile AA' mapped on the figure 4.1 showing the Base Cretaceous Unconformity, which was mapped using jump correlation method, and salt diapirs.*

5. Seismic interpretation and results

5.1 Overview of the interpreted seismic horizons

In order to get the full understanding of how the surface of the Nordkapp Basin evolved during the Cretaceous Period, there are mapped two main horizons in this work: the Top Cretaceous Boundary and the Base Cretaceous Unconformity which outline the Cretaceous Period in the Nordkapp Basin. There is also mapped a less prominent reflector R1, which is located between them.

The Jurassic – Cretaceous boundary is defined as the Base Cretaceous Unconformity (BCU) (Marin et al., 2017). The BCU is well defined on seismic data (figure 4.8, figure 5.1, and figure 5.2). This strong reflection is the result of a significant difference in acoustic impedance across the boundary between the lithological layers. The reflector is continuous and is present along the whole basin excluding the tops of the diapirs.

The upper boundary of the Cretaceous Period in the Nordkapp basin is in large areas represented by the Upper Regional Unconformity (URU). As the result, in such areas the Top Cretaceous horizon, which is defined in this study as a boundary between the Cretaceous and Paleogene, is not present and the uppermost preserved Cretaceous layers which can be found there are the layers, which were not removed by the massive glacial erosion in the Pliocene-Pleistocene. Such layers were deposited earlier than the Top Cretaceous horizon and do not correspond to the layers deposited during the Late Cretaceous. In the places, where the boundary between the Upper Cretaceous and Paleogene is present and was not removed by the glacial erosion, the Top Cretaceous Boundary (TCB) (Figure 5.2) is mapped based on interpretation made by NPD (NPD, 2014b). In areas where the TCB is preserved, the reflector is strong and is well seen on seismic (figure 5.2).

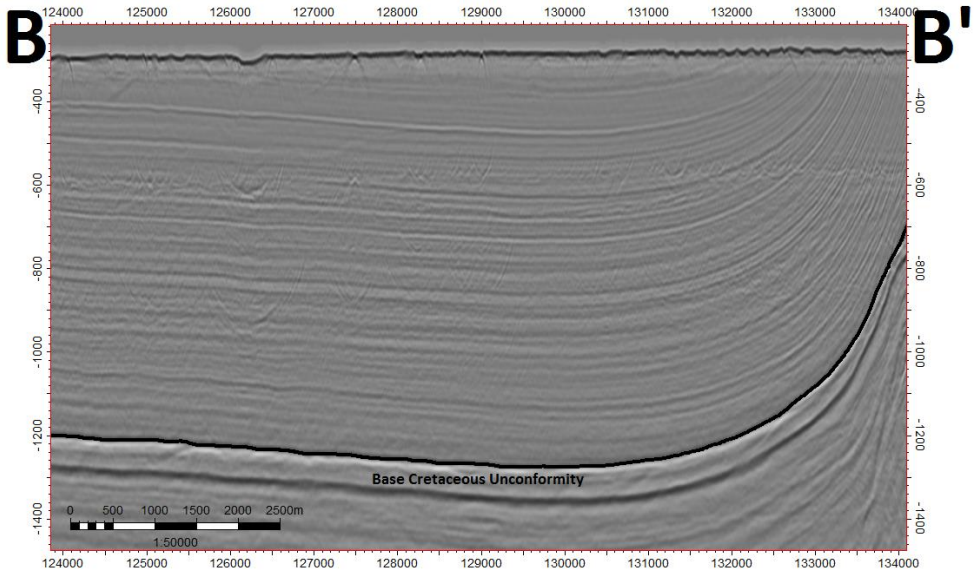

Figure 5.1: *Seismic profile BB' mapped on the figure 4.1 showing Base Cretaceous Unconformity.*

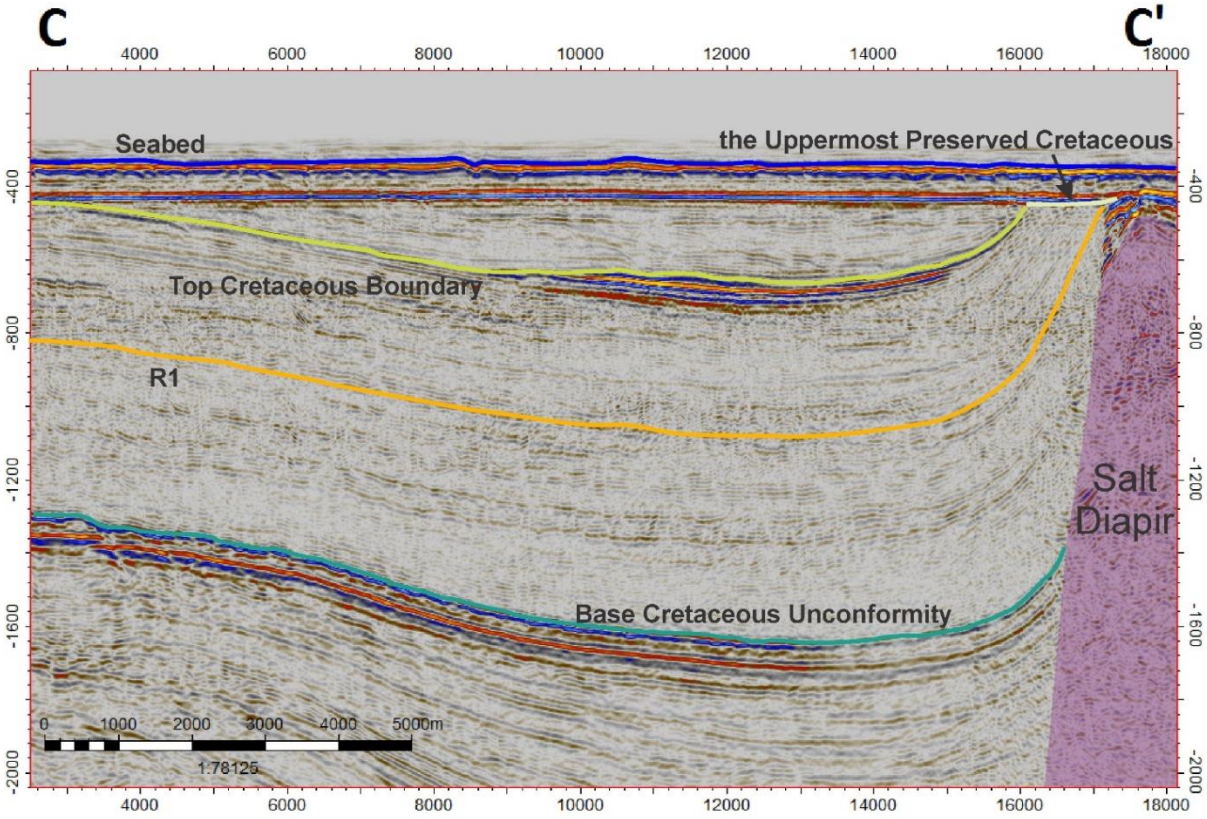

Figure 5.2: *Seismic profile CC' showing Top Cretaceous Boundary, boundary of the uppermost preserved Cretaceous, Base Cretaceous Unconformity and a salt diapir. Position of the profile is shown on figure 4.1.*

In addition to the two bounding reflectors (BCU and TCB), the internal horizon R1 within the Cretaceous has been interpreted (figure 5.2). The reflection is partly continuous and is present in some parts of the basin. Moreover, due to low resolution and distortion of the seismic signal

it is hard and sometimes impossible to accurately map the reflector. However, on large scale profiles it is still visible and its interpretation helps to understand geologic development of the Nordkapp Basin.

5.2 Seismic to well correlation

The reflectors mapped in this work are correlated to the five wells described in section 4.1. The position of the wells is shown on the figures 4.2 and 5.3. A composite seismic profile DD' though the all available wells is made (figure 5.3, figure 5.4). Depth in wells of the mapped horizons is present in the table 5.1.

Seismic profile DD' (figure 5.4) illustrates that the Top Cretaceous horizon is present only in the areas inside the southern part of the Nordkapp Basin. Due to this, the Top Cretaceous horizon as defined here is not present in most of the wells available for this thesis. The uppermost preserved Cretaceous layers which follow the line of the Upper Regional Unconformity are expected to be found in the rest of the wells. R1 reflector is also only partly presented in the Nordkapp Basin (figure 5.4).

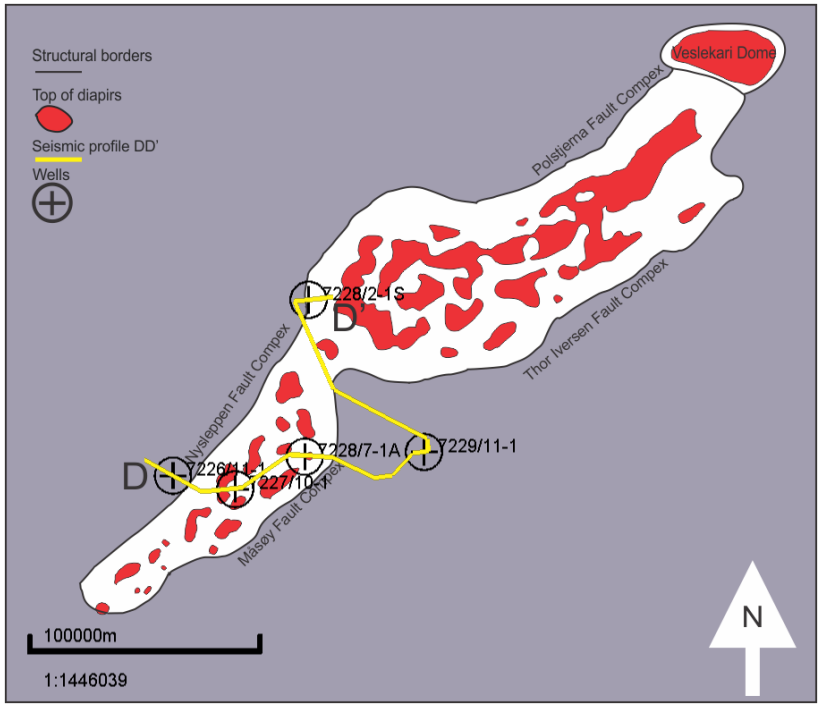

Figure 5.3: *A scheme of the Nordkapp Basin, showing seismic profile DD' and correlated wells. Profile itself is shown on figure 5.4.*

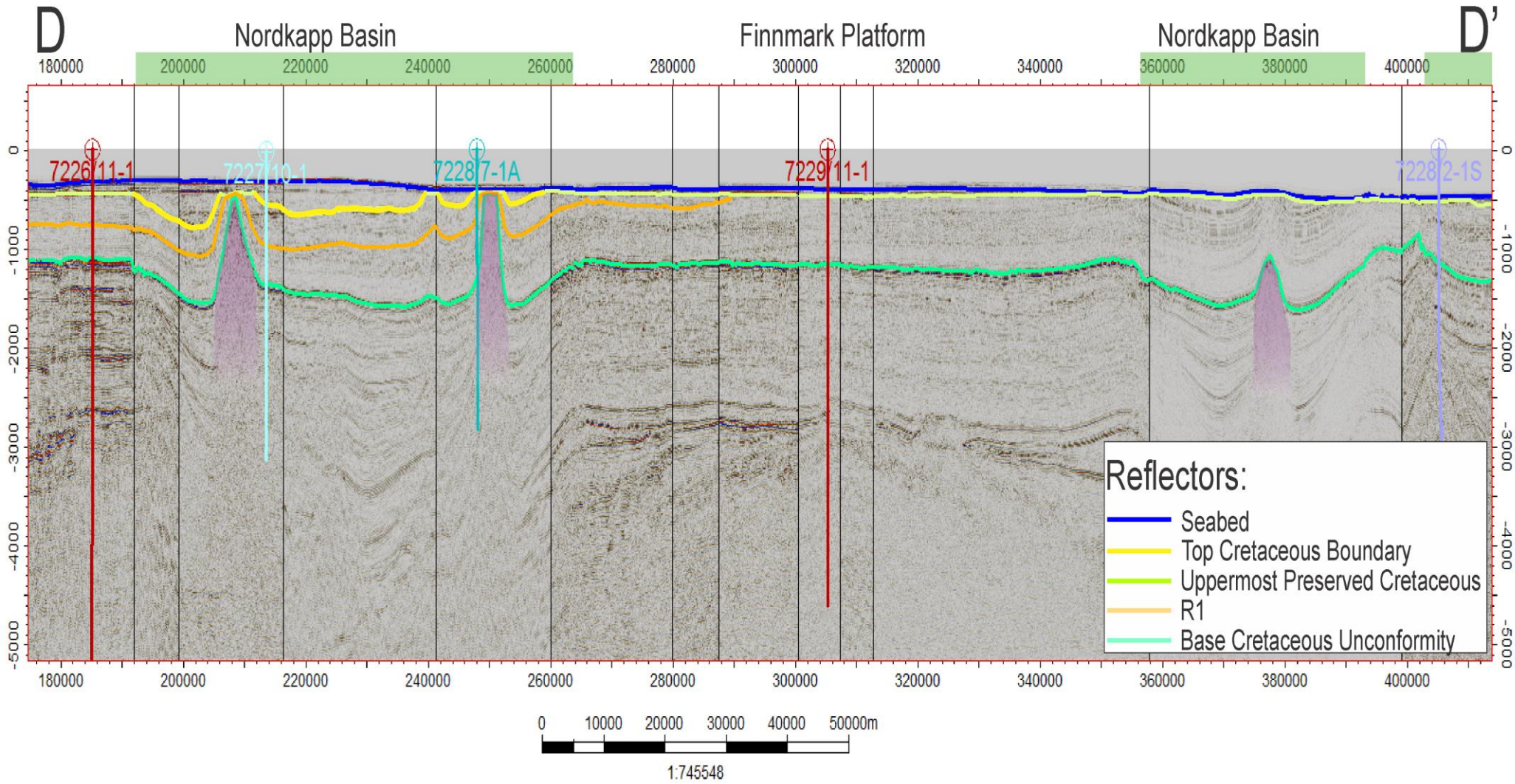

Figure 5.4: *Seismic profile DD' showing reflectors and wells correlated in this thesis. Position of the profile is shown on the figure 5.3. Area inside the Nordkapp Basin is highlighted in green. Diapiric structures and their artefacts which interrupt the Cretaceous reflectors, are highlighted in purple. Profile is composite and consists of seismic lines (from left to right): BARE05-D-14-84, D-14-84B_R05, BARE02-7210-B, NBGS-90-214, NBGS-90-424, BARE02-D-3, GNB-87-126, BARE02-D-11, SH8810-209, SG8737-106, BARE02-D-1, NBR06-259202 and MN89-601.*

Correlation to well 7226/11-1 (figure 5.5) shows that the Base Cretaceous Unconformity corresponds with the base of the Cretaceous limestones and claystones and top of the Jurassic organic rich shales represented by the Hekkingen Formation. The upper boundary the Knurr Formation is found at of 1141-meter depth and the base is at 1147-meter depth (true vertical depth with rotary kelly bushing as a reference point is used here and below). The thickness of the formation is below seismic resolution. The seismic signal spreads through overlying Kolmule Formation, which bottom is at 1141-meter depth, and does not react significantly on the Knurr Formation. As the result, the acoustic impedance contrast seen on seismic is the contrast between the Kolmule Formation and the Hekkingen Formation. The depth of reflector R1 is 698 meters and corresponds to middle of the Kolmule Formation (Albian). The boundary of the uppermost preserved Cretaceous layers is at 374-meter depth and is present with the eroded top of the Kolmule Formation.

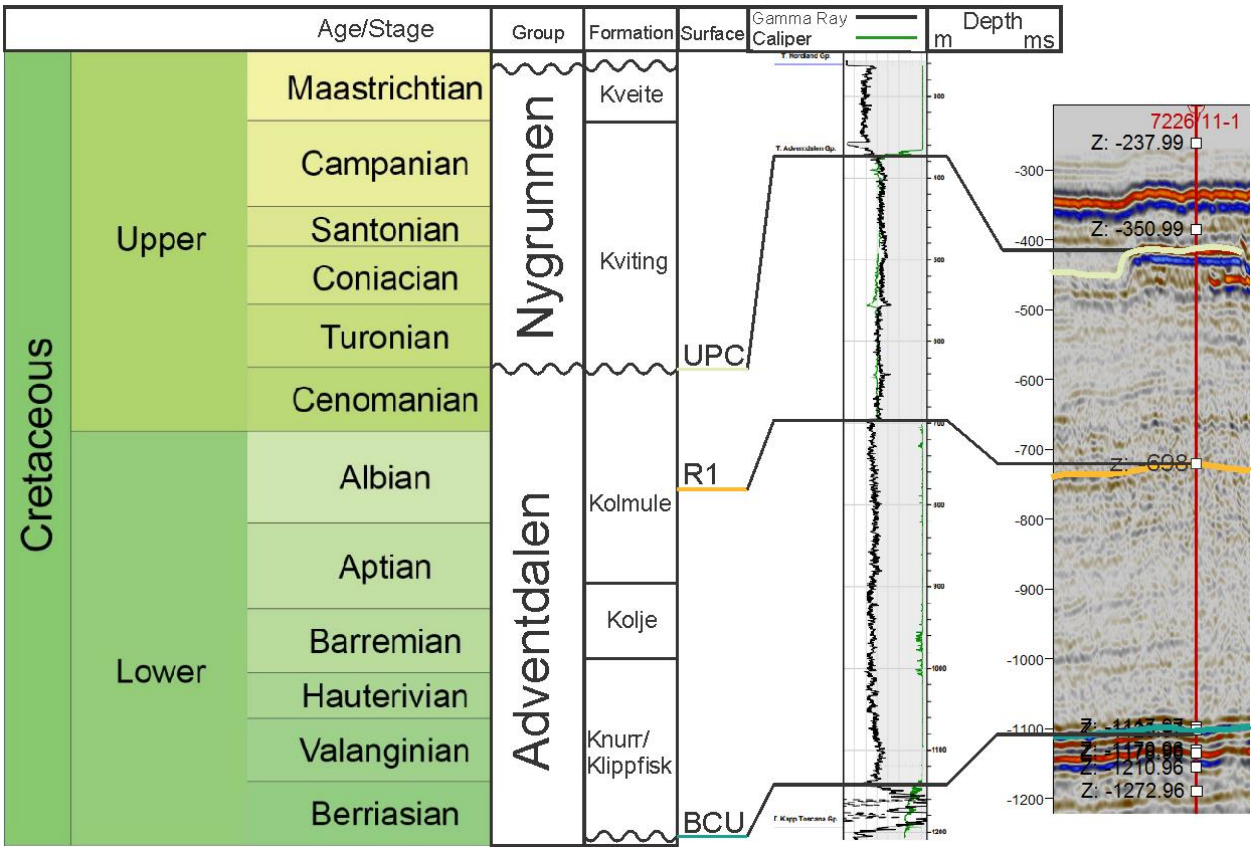

Figure 5.5: *Seismic to well correlation for well 7226/11-1. The well is located on the Bjarmeland Platform (Norsel High) west to the Nordkapp Basin (figure 4.2, figure 5.3). UPC – the boundary of the uppermost preserved Cretaceous, BCU – Base Cretaceous Unconformity. True vertical depth is used in well logs.*

Seismic correlation to well 7227/10-1 (figure 5.6) shows that Top Cretaceous horizon is correlated with the top of the Nygrunnen Group, represented by the Kviting formation of Campanian Age, and is in the well at a depth of 513 meters. The Kveite Formation is not present in the well. R1 reflector is observed in the seismic data, but is not easily recognized in the well logs, including Gamma ray log. This can be described by relatively the same mineral composition of the Albian Part of the Komlule Formation in the well due to constant depositional source during the time of deposition (Smelror et al., 2009). The depth of R1 reflector is in well 7227/10-1 correlated to 1027 meters. The Base Cretaceous Unconformity in this well is correlated with Bottom of Adventalen Group and corresponds to the contrast between the Hekkingen and the Stø formations (figure 5.6). The Fuglen Formation is only 2-meter-thick, so it cannot produce noticeable seismic signal, and is "masked" by signal set up by the boundary between the Hekkingen and the Stø formations. The base of the Adventalen Group is found at 1539 meters, correlating to about 1300 milliseconds (TWT) in the seismic data. The Cretaceous-Jurassic boundary is not easily recognized in seismic data and is not seen as a part of BCU reflector. This can be explained by low seismic resolution and nearly the same acoustic impedance of the Hekkingen and the Lowest Cretaceous formations in this area. It has depth of 1472 meter or 1260 milliseconds. The difference in 67 meters or 40 milliseconds between the real base of the Cretaceous deposits and BCU is bigger than seismic resolution, but still is quite small. However, the difference in stratigraphic age is more than 20 million years.

Seismic correlation to well 7228/7-1A (figure 5.7) is influenced by the adjacent salt diapir. Well 7228/7-1A did not penetrate the salt, but the salt structures influence and diffract seismic signals, making it difficult to correlate seismic data with well logs. However, both well logs and seismic data show that the Top Cretaceous Boundary is not present in the well, so the uppermost preserved Cretaceous layers corresponds to the top of the Kolmule Formation or the top of the Adventdalen Group at a depth of 334 meters. The reflector of the Base Cretaceous Unconformity is correlated to the base of the Knurr formation (1314-meter depth). The thickness of the Knurr formation (14 meters) is at the point of seismic resolution. The formation is still recognizable in the seismic data, but as a single reflection. This single reflection is influenced by the difference in acoustic impedance between the Kolmule and the Hekkingen formations. Reflector R1 is also distorted on the seismic profile, but is present in

the well and is barely recognizable on Gamma ray log. Its depth is found at 626 meters, which corresponds to Albian part of the Kolmule Formation.

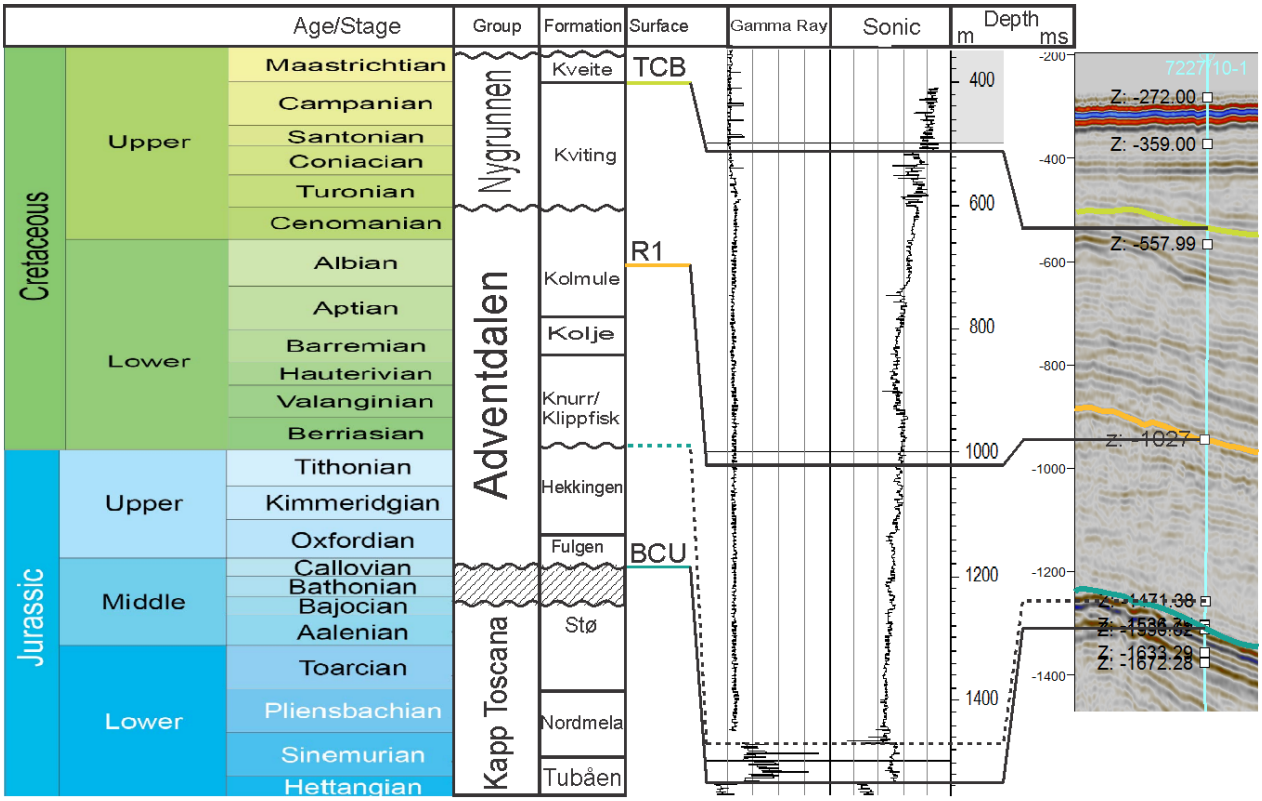

Figure 5.6: *Seismic to well correlation for well 7227/10-1. The well is located in the southwest part of the Nordkapp Basin (figure 4.2, figure 5.3). TCB – Top Cretaceous Boundary, BCU – Base Cretaceous Unconformity, dotted line the same colour as BCU – the Cretaceous-Jurassic boundary. True vertical depth is used in well logs.*

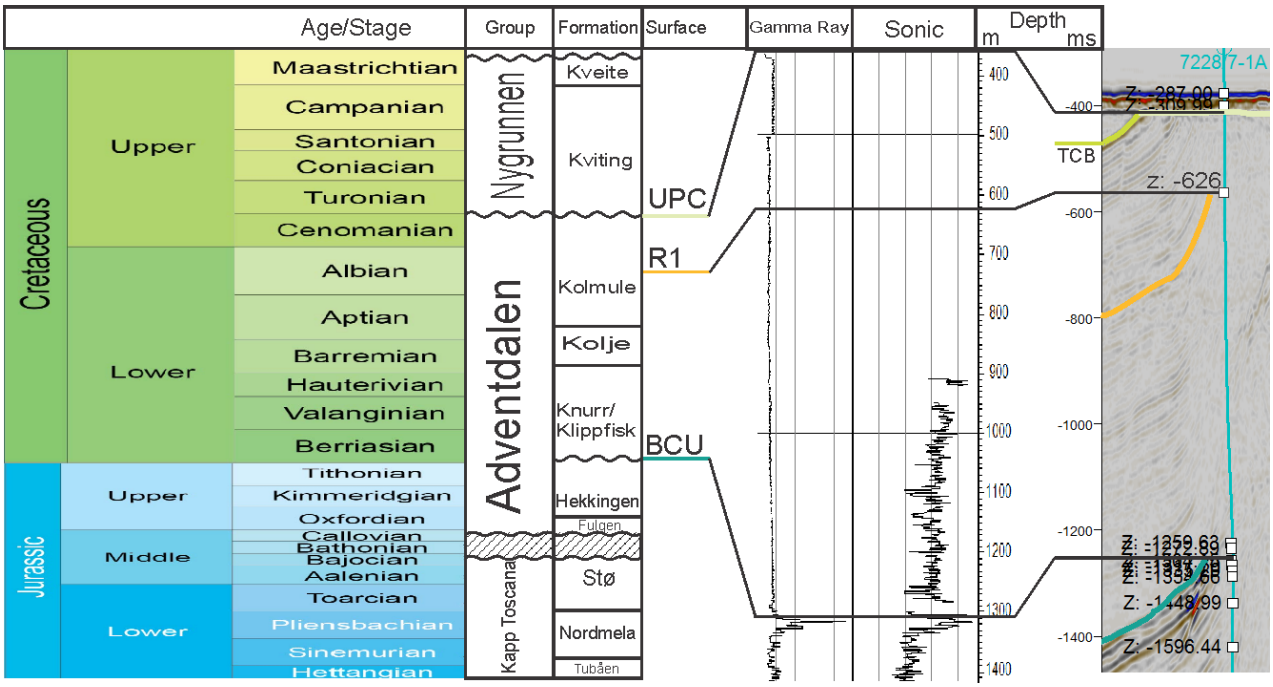

Figure 5.7: *Seismic correlation for well 7228/7-1A. The well is located in southwest part of the Nordkapp Basin, 14 km west from the Måsøy Fault Complex (figure 4.2, figure 5.3). UPC – the boundary of the uppermost preserved Cretaceous layers, BCU – Base Cretaceous Unconformity, TCB – Top Cretaceous Boundary (is not present in the well, but is seen nearby on seismic profile. True vertical depth is used in well logs.*

The Top Cretaceous reflector as defined in this study is not present in well 7229/11-1. Seismic correlation for the well (figure 5.8) shows that the uppermost Cretaceous sediments are presented by the Kolmule Formation, which if found at 379 meters and have an age of Late Cenomanian. The Base Cretaceous Unconformity is correlated with the base of Knurr Formation or the top of the Hekkingen Formation, in the well found at depth of 1212 meters. However, the Knurr Formation is too thin (12 meter) to be visible on seismic, so the reflection observed is believed to represent the seismic impedance contrast between Kolmule and Hekkingen formations.

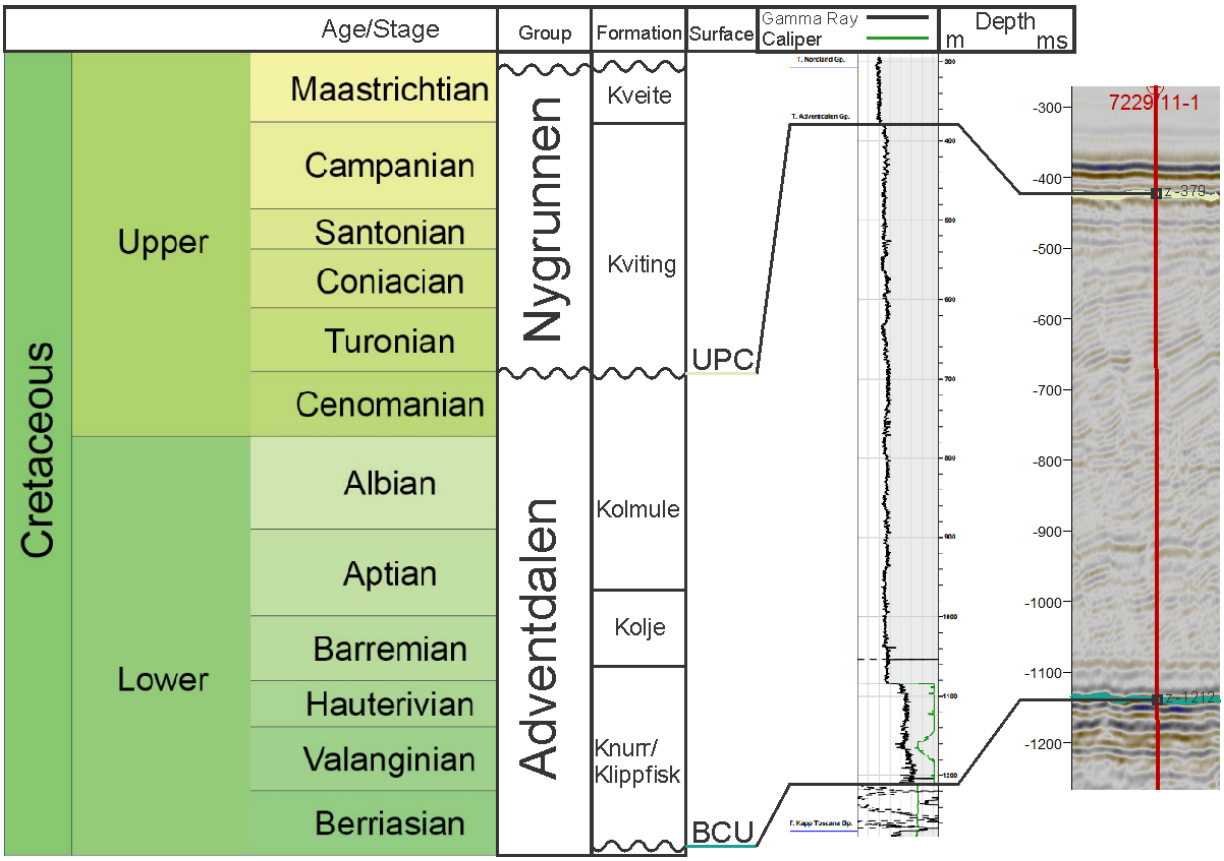

Figure 5.8: *Seismic correlation for well 7229/11-1. The well is located on the Finnmark Platform 30 km southeast to the Nordkapp Basin. UPC – the boundary of the uppermost preserved Cretaceous layers, BCU – Base Cretaceous Unconformity. True vertical depth is used in well logs.*

The Top Cretaceous horizon as defined in this work is not present in well 7228/2-1S. Seismic correlation to the well (figure 5.9) shows that the youngest Cretaceous layers are present with the Kolmule Formation. The eroded top of the formation is found at depth of 373 meters. Reflection from the Base Cretaceous Unconformity is correlated with the base of the Knurr Formation, which has depth of 1168 meters. The Knurr Formation in this area is thick enough to produce a reflection visible on seismic both at the top and at the base of the formation. The top is 1110 meters beneath the seafloor and thickness of the formation is 48 meters in the well which is bigger, than vertical resolution of the seismic dataset used to map the reflectors in this area (~42 meters, dominant frequency ~13 Hz) (see section 4.2).

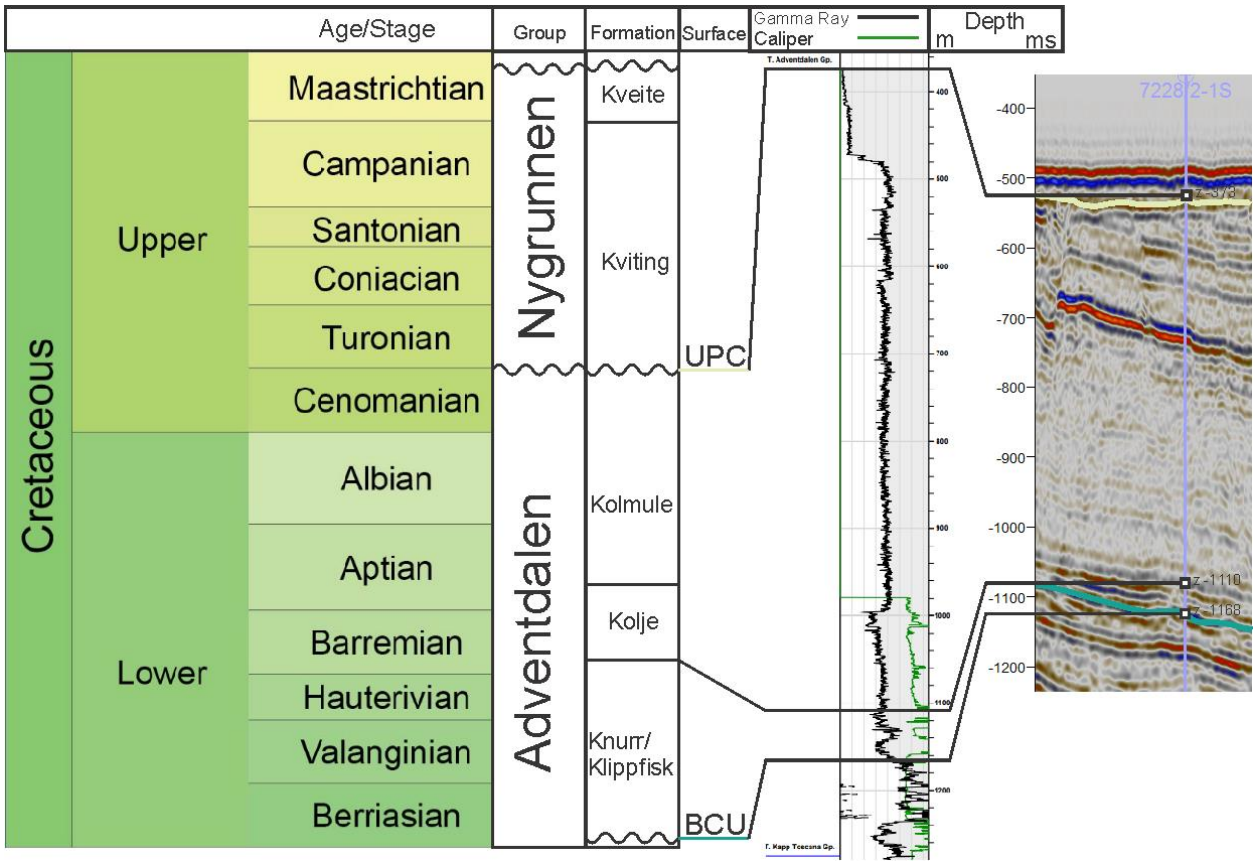

Figure 5.9: *Seismic correlation for well 7228/2-1S which was drilled on the western margin of the Nordkapp Basin close to Nysleppen Fault Complex. Location for the well is shown on the figures 4.2 and 5.3. UPC – the Uppermost Preserved Cretaceous layers, BCU – Base Cretaceous Unconformity. Top of the Knurr Formation is also correlated to well logs and seismic. True vertical depth is used in well logs.*

Looking through the seismic correlation to wells 7226/11-1, 7227/10-1, 7228/7-1A, 7229/11-1 and 7228/2-1S (figures 5.5-5.9) it is not difficult to notice that the Base Cretaceous Unconformity in most cases is correlated with base of the Knurr Formation (where it is present) or the Kolmule Formation. These two formations are considered as the Lowest Cretaceous intervals present in the study area. The formation which usually is found below BCU is the Hekkingen Formation – the youngest Jurassic interval present in the basin. BCU is found at the boundary between these two Mesozoic periods. It should be mentioned, that in one of the wells 7227/10-1 (figure 5.6) BCU is correlated with the base of the Adventdalen Group (base of the Fuglen formation) and the Stø Formation is below it, but this is explained by insufficient resolution of the seismic data and noise. The depth of the Base Cretaceous in the wells varies from 1141 to 1472 meters and its top varies from 334 to 379 meters in the wells where the Nygrunnen Group of the Upper Cretaceous is not present. The boundary of the uppermost preserved Cretaceous layers simply follows the eroded line of the Upper

Regional Unconformity. The boundary between the Upper Cretaceous and the Paleocene sediments is present only in the well 7227/10-1 (figure 5.6) and has depth of 513 meters. These are the youngest Cretaceous sediments found in all the wells available for this study. These sediments correspond to the Kviting Formation and are present in the south part of the Nordkapp Basin. The oldest Cretaceous sediments are found in wells 7226/11-1 (figure 5.5), 7228/7-1A (figure 5.7) and 7229/11-1 (figure 5.8) and 7228/2-1S (figure 5.9) and are present by the Knurr Formation. The Knurr Formation thinners in south-west direction inside the Nordkapp Basin and as a result is not present in the southernmost well available for this study (7227/10-1) (figure 5.6). In addition, it should be mentioned that the Kolje Formation is not present in the wells at all, so the Cretaceous deposits in the study area are present mostly by the Kolmule Formation and in some areas also by the Knurr and Kviting formations, which are way thinner than the massive Kolmule Formation. R1 reflector is present in three wells: 7226/11-1 (figure 5.5), 7227/10-1 (figure 5.6) and 7228/7-1A (figure 5.7). Its depth in the wells varies from 626 to 698 meters and its stratigraphic age corresponds to the Mid Albian. The brief overview of the correlated reflectors is present in the table 5.1

Reflector / Well	7226/11-1	7227/10-1	7228/7-1A	7229/11-1	7228/2-1S
Eroded boundary of uppermost preserved Cretaceous	374 m	-	334 m	379 m	373 m
Top Cretaceous Boundary	-	513 m	-	-	-
R1	698 m	1027 m	626 m	-	-
Base Cretaceous Unconformity	1147 m	1539 m	1314 m	1212 m	1168 m

Table 5.1: *Depth of the mapped reflectors in the wells.*

5.3 Constructed maps and surfaces

The outline of the Nordkapp Basin is given in Figure 5.10 with regional seismic profile EE' (figure 5.11) along the whole Nordkapp Basin and profiles FF' (figure 5.12) and GG' (figure 5.13).

5.3.1 Base Cretaceous Unconformity

Figure 5.10: *Scheme of the Nordkapp Basin showing seismic profiles EE', FF' and GG'.*

The Base Cretaceous Unconformity is the main and the strongest reflector (except the seabed) which is interpreted during this study.

Seismic profile EE' (figure 5.11) illustrates that the Base Cretaceous Unconformity is present within the whole Nordkapp Basin. The depth to the horizon shows a slight increase from the north to the south part of the basin in the places, especially where the reflector is not influenced by the salt diapirism. Faults are distinguishable on the both ends of the profile.

On the seismic profile FF' (figure 5.12) the depth to the BCU varies from 1100 ms TWT to 1250 ms TWT where the salt structures are not present. The reflector reaches its maximum depth in the sub-basin between the two salt domes in the middle part of the profile which corresponds to the middle of the north part of the Nordkapp Basin (figure 5.10).

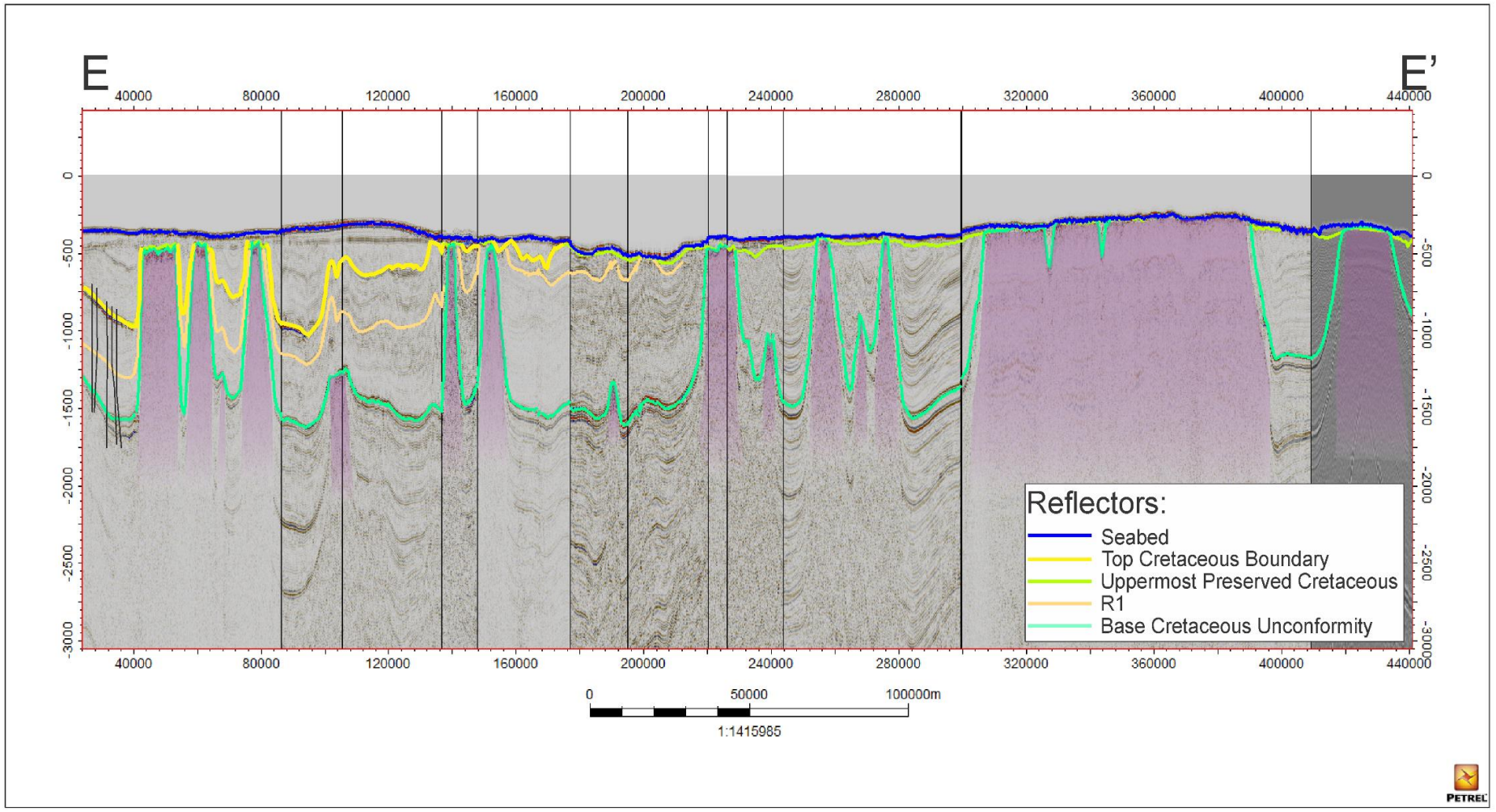

Figure 5.11: *Seismic profile EE' along the whole Nordkapp Basin showing reflectors interpreted in this thesis. Position of the profile is shown on the figure 5.10. Diapiric structures which interrupt the Cretaceous stratigraphy, are highlighted in purple.*

There are no marginal faults on the western part of the profile FF'. However, on the east side of FF' profile there are distinguishable faults (north part of the Thor Iversen Fault Complex).

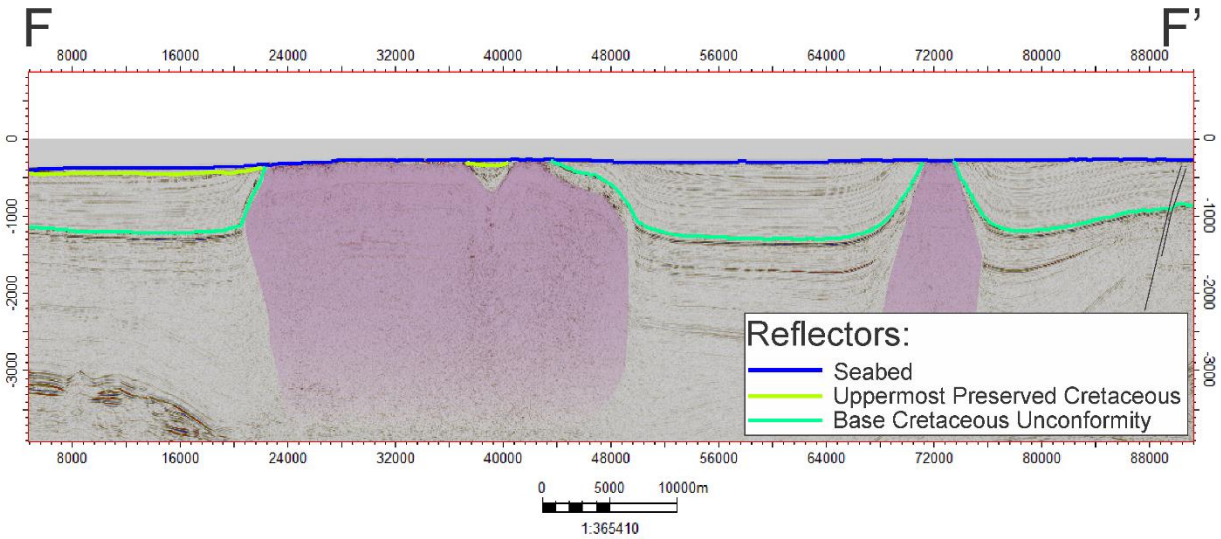

Figure 5.12: *Seismic profile FF' across the north part of the Nordkapp Basin. Position of the profile is shown on the figure 5.10. Diapiric structures are highlighted with purple.*

On the GG' profile across the south part of the Nordkapp Basin (figure 5.13) the BCU reflector is deeper than on the profile FF'. Its depth in the basin varies from 1300 to 1500 ms TWT. The reflector reaches its maximum depth in the sub-basin in the middle of the profile.

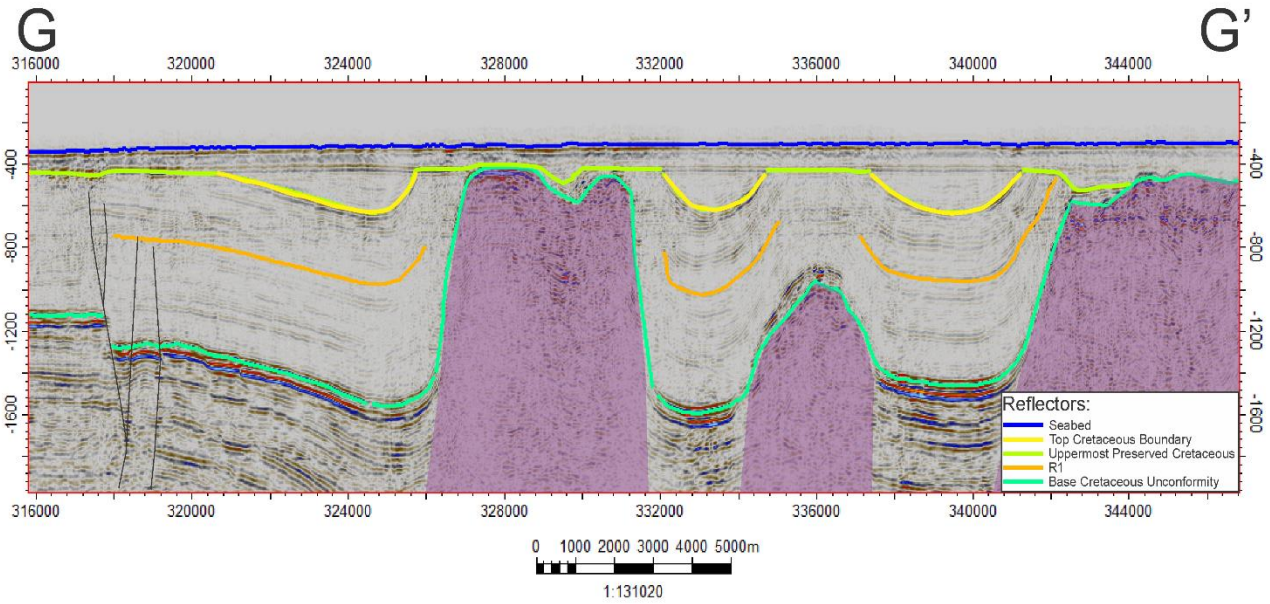

Figure 5.13: *Seismic profile GG' across the south part of the Nordkapp Basin. Position of the profile is shown on the figure 5.10. Diapiric structures are highlighted with purple.*

On the west side of the GG’ profile clear faulting is observed to influence the BCU. The same fault is visible on the profile CC’ (between 3000 and 4000 meters) (figure 5.2) which is several kilometers north to GG’ profile. Moreover, on the seismic profile DD’ (figure 5.4) the fault is also visible in the interval between 390000 and 410000 meters in the northern part of the profile, near 190000 meters in the southern part of the profile (figure 5.4), which corresponds to the northern and southern parts of the Nysleppen Fault Complex.

On the seismic profile DD’ (5.4), faults of the Måsøy Fault Complex are clearly seen on seismic as a sharp discontinuity on the eastern flank of the south part of the basin between 260000 and 280000 meters and between 350000 and 360000 meters on the DD’ profile (figure 5.4).

A 3D surface of the BCU is given (figure 5.14). The depth of the horizon varies from 1100-1200 ms TWT to 1600-1700 ms TWT, where the reflector is not interrupted by salt diapirs. The depth of the BCU increases from the northeast part of the basin to its southwest. This gradient is clearly seen on the profile EE’ with the flattened BCU reflector (figure 5.15). Fault complexes controlling the basin are clearly seen on the time-structure map (figure 5.15).

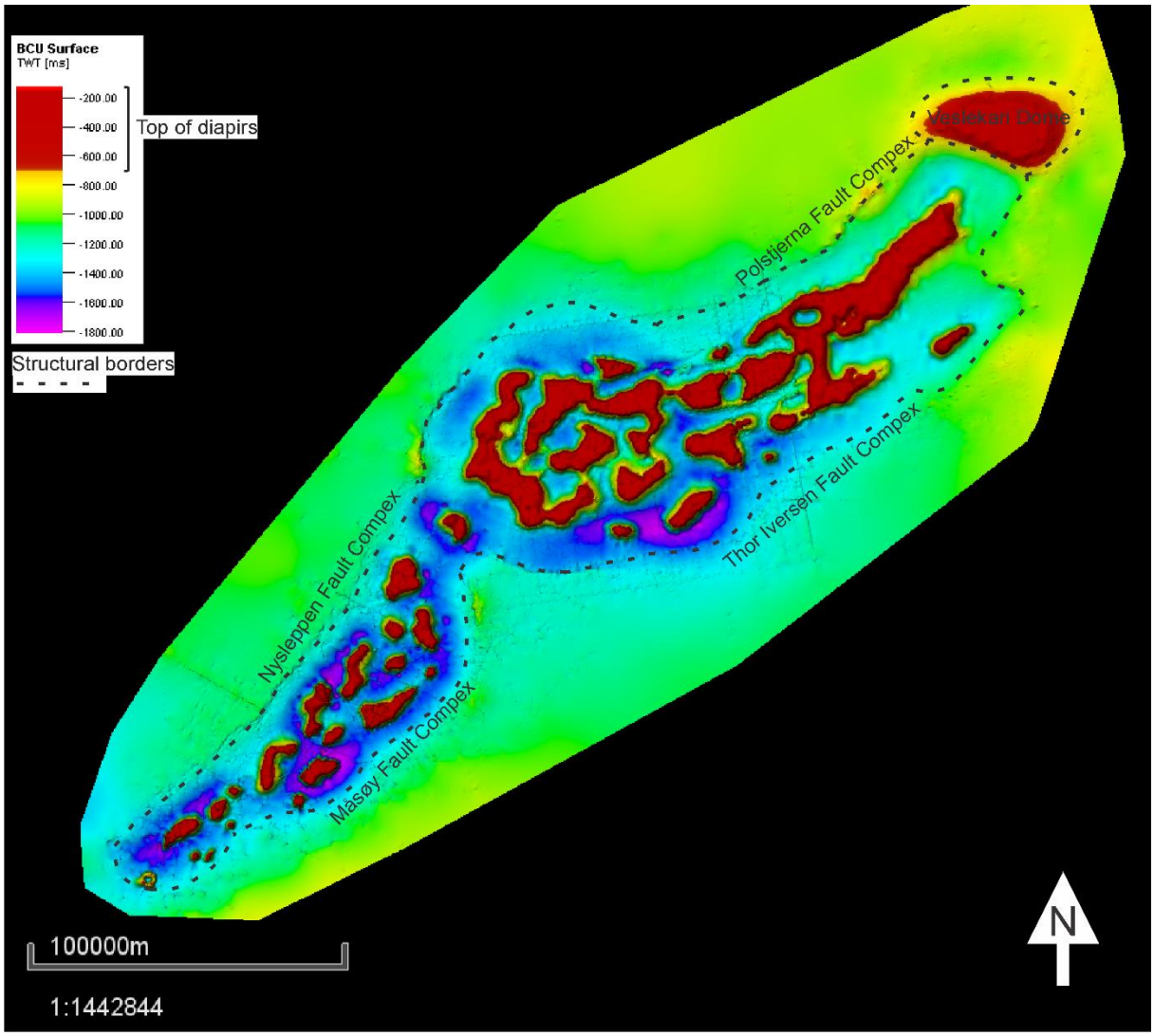

Figure 5.14: *Time-structure map of the Base Cretaceous Unconformity and diapirs in the Nordkapp Basin and nearby structures. Vertical exaggeration of 5 is used.*

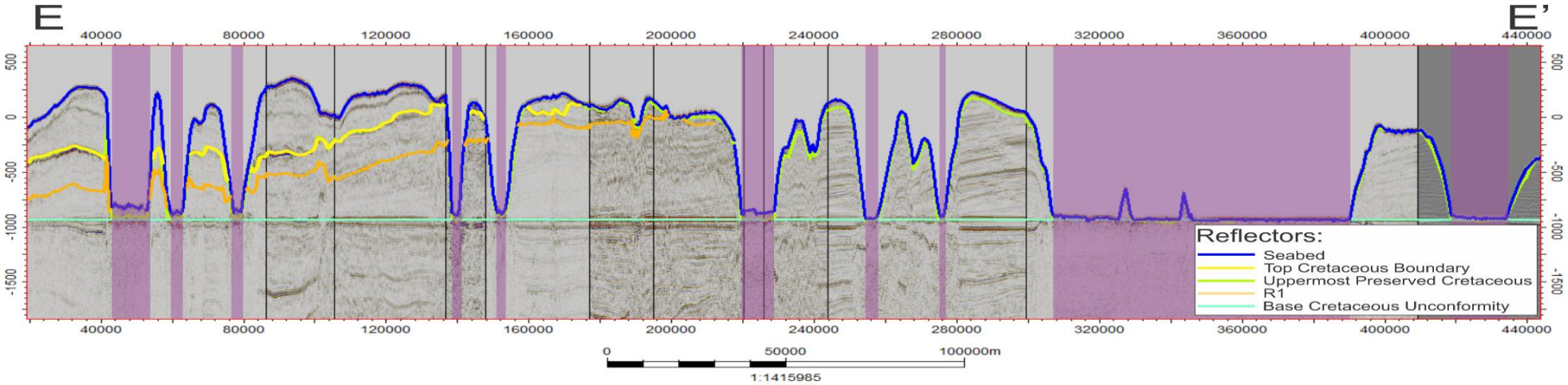

Figure 5.15: *Seismic profile EE' which is flattened according to the reflector of the Base Cretaceous Unconformity. Diapiric structures are highlighted with purple. Position of the profile is shown on the figure 5.10.*

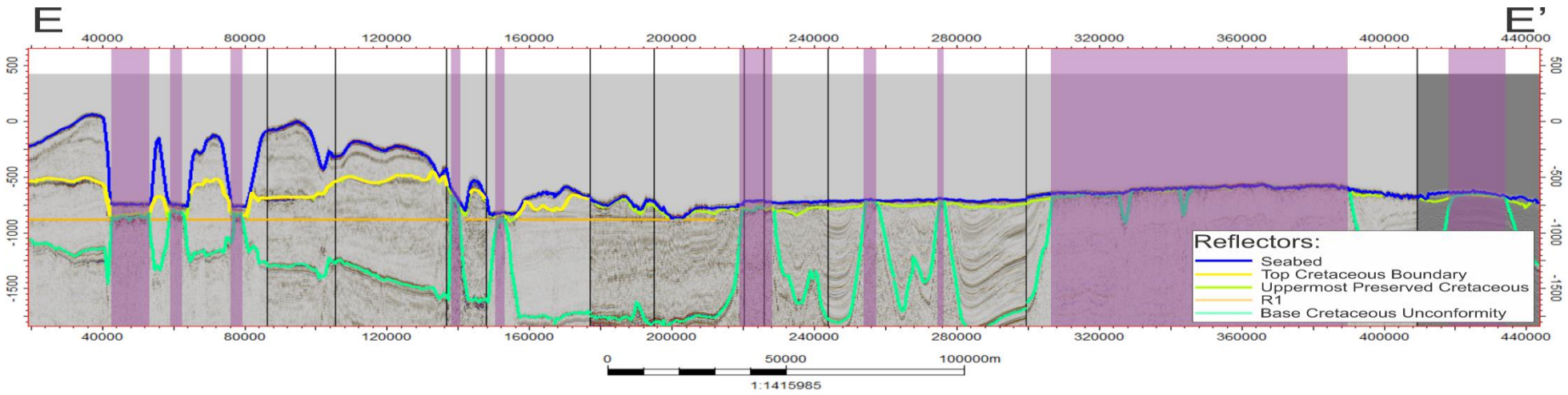

Figure 5.16: *Seismic profile EE' which is flattened according to the R1 reflector. Diapiric structures are highlighted with purple. Position of the profile is shown on the figure 5.10.*

5.3.2 R1 horizon

Profile EE’ (figure 5.11) illustrates that the R1 horizon is present only in the south part of the Nordkapp Basin. Its depth along the basin on the profile increases from near 600 ms TWT in the middle of the basin to 1300 ms TWT in the southern part. The dip of the reflector appears steeper than that of BCU. This is especially seen on version of the EE’ profile which is constructed using R1 or the BCU as a horizontal axe (figure 5.15, figure 5.16). Discontinuities of the reflector, caused by the fault presence, are seen on the south part of profile EE’ (figure 5.11).

There is an absence of the reflector on the FF’ profile (figure 5.12) and its presence on the GG’ profile (figure 5.13). The lateral depth of the reflector varies from 700 ms TWT on the flanks of the basin, to 900 ms TWT in the sub-basins between the salt domes on the profile GG’ (figure 5.13). The sharp break-up of the reflection is visible at the western boundary of the basin (figure 5.13). This discontinuity follows the major faults of the Nysleppen Fault Complex. Moreover, on the DD’ profile (figure 5.4) the discontinuities related to faults are seen in the interval between 260000 and 280000 meters, which corresponds to the eastern flank of the south part of the Nordkapp Basin and the Måsøy Fault Complex.

The 3D map of the R1 horizon (figure 5.17) illustrates the outline of the horizon in the Nordkapp Basin. The shallowest part of the horizon is situated the middle part of the basin. The influence of the erosion events is seen on the map as there are parts of the horizon, which are not connected to each other. The total dipping of the reflector from the north to the south is also easily seen on the map (figure 5.17). The depth of the reflector increases from 500-600 ms TWT on its erosion boundary to 1200-1300 ms TWT in the southern part of the Nordkapp Basin. The sharp borders of the Nordkapp Basin are present in the north part of the reflector, however in the southern part they are smoother. Nevertheless, the average trend of the inclination and dipping of the horizon is preserved and is visible on the map.

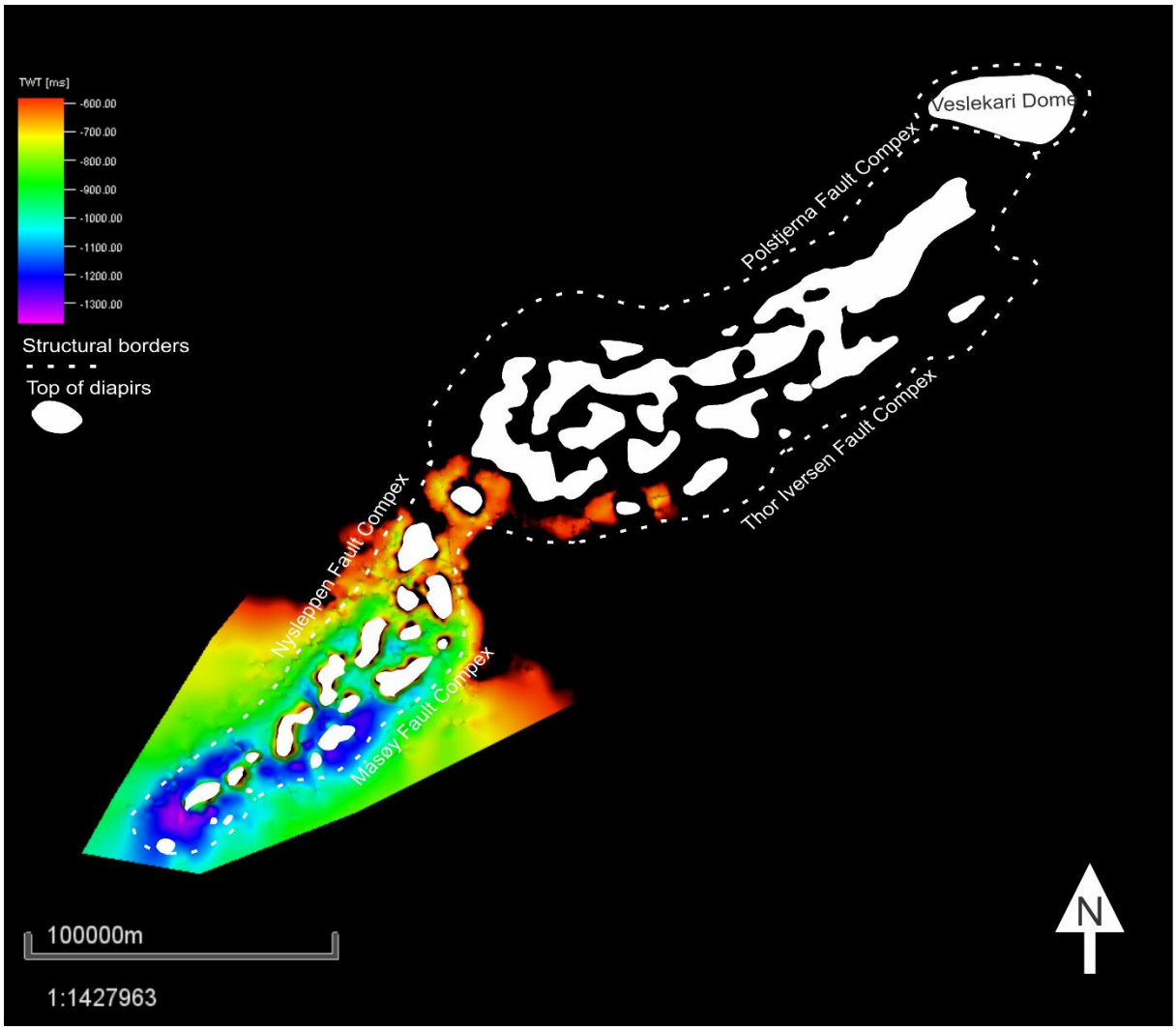

Figure 5.17: *Map of the R1 seismic horizon and salt diapirs in the Nordkapp Basin and nearby structures. Vertical exaggeration of 5 is used.*

5.3.3 Top Cretaceous

Seismic profile EE' (figure 5.11) shows that the base Paleogene is only present in the southern part of the basin. The north erosion edge of the Top Cretaceous Boundary is at near 500 ms TWT depth 36 km south to the northern edge of R1 reflector (the north erosion edge of R1 is at ~212 km on the seismic profile EE' (figure 5.11) and the north erosion edge of the TCB is at ~176 km). The northern truncation edge of the TCB is especially seen on the version of the EE' profile where the TCP is flattered (figure 5.19). The reflector reaches its maximum depth of 950-1000 ms in the sub-basins between the salt diapirs. The slope of the TCB reflector is in most cases identical to the slope of the R1 reflector. This is especially seen on the EE' profile where the BCU reflector is set as a horizontal axe (figure 5.15). Step-like discontinuities are

barely seen in the south part of the profile because the major faults are not developed in the sequences above the R1 reflector, but the minor faults are still present in the southern boundary of the Nordkapp Basin. The reflector of the uppermost preserved Cretaceous boundary in most cases follows the erosion boundary of the Upper Regional Unconformity reflector. However, there are a few small spots, where the boundary of the uppermost preserved Cretaceous does not correspond to the Upper Regional Unconformity. This can be described by the occurrence of the minor erosion events before URU was established.

On the GG' profile (figure 5.12), the Top Cretaceous Boundary as defined in this study is not present, because the profile is too north from the erosion edge of the Top Cretaceous reflector. However, the boundary of the uppermost preserved Cretaceous is present and follows the line of URU. The Top Cretaceous Boundary is clearly seen on the seismic profile FF' (figure 5.13,) which is made across the south part of the Nordkapp Basin. The maximum depth the reflector reaches on the profile is 500 ms.

A difference between the Top Cretaceous Boundary and the erosion boundary of the uppermost preserved Cretaceous (the Upper Regional Unconformity) is especially seen on the profiles CC' (figure 5.2) and FF' (figure 5.13). The reflectors differ not only in the strength of the seismic signal, but also in the types of seismic facies they divide. On seismic profile DD' (figure 5.4), which is made across the south part of the Nordkapp Basin, is visible how the Nysleppen Fault Complex affects the TCB horizon (near 192000 m on the profile (figure 5.4)). The TCB truncated edge is in the same place, where the marginal faults are present, and west to it the Upper Cretaceous sediments are fully removed by the Pliocene-Pleistocene erosion.

The same toplap can be observed on the east side of the basin on the DD' profile near 260000 m (figure 5.4). The truncated edge of the Top Cretaceous reflector is near the eastern margin of the basin and the reflector is eroded outside of the basin.

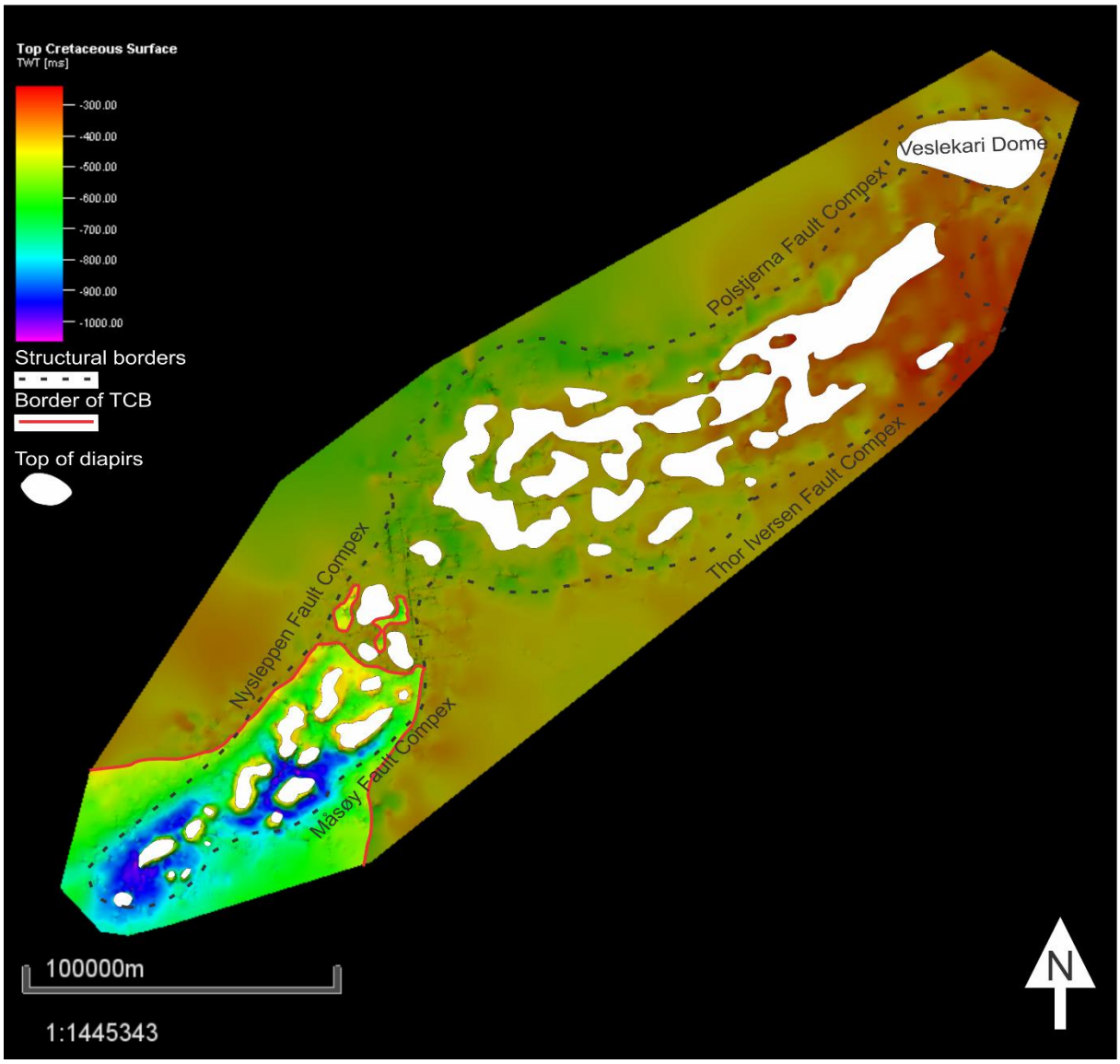

Figure 5.18: *Time-structure map of the Top Cretaceous Boundary in the Nordkapp basin and nearby structures. The areas where the Top Cretaceous Boundary is removed by erosion events are shadowed and the uppermost preserved Cretaceous / Upper Regional Unconformity is showed there. Vertical exaggeration of 5 is used.*

The 3D time-structure map of the Top Cretaceous (figure 5.18) illustrates the erosion edges of the TCB. Moreover, there can be seen major faults of the Nysleppen and Måsøy fault complexes. The depth varies from 300 ms TWT to more than 900 ms TWT in places where the horizon is not penetrated by salt diapirs. Note, that the Base Paleogene boundary is preserved only in the southwest part of the basin and in the other areas only the erosion boundary of the Upper Regional Unconformity divides the preserved Cretaceous intervals from the Quaternary sediments.

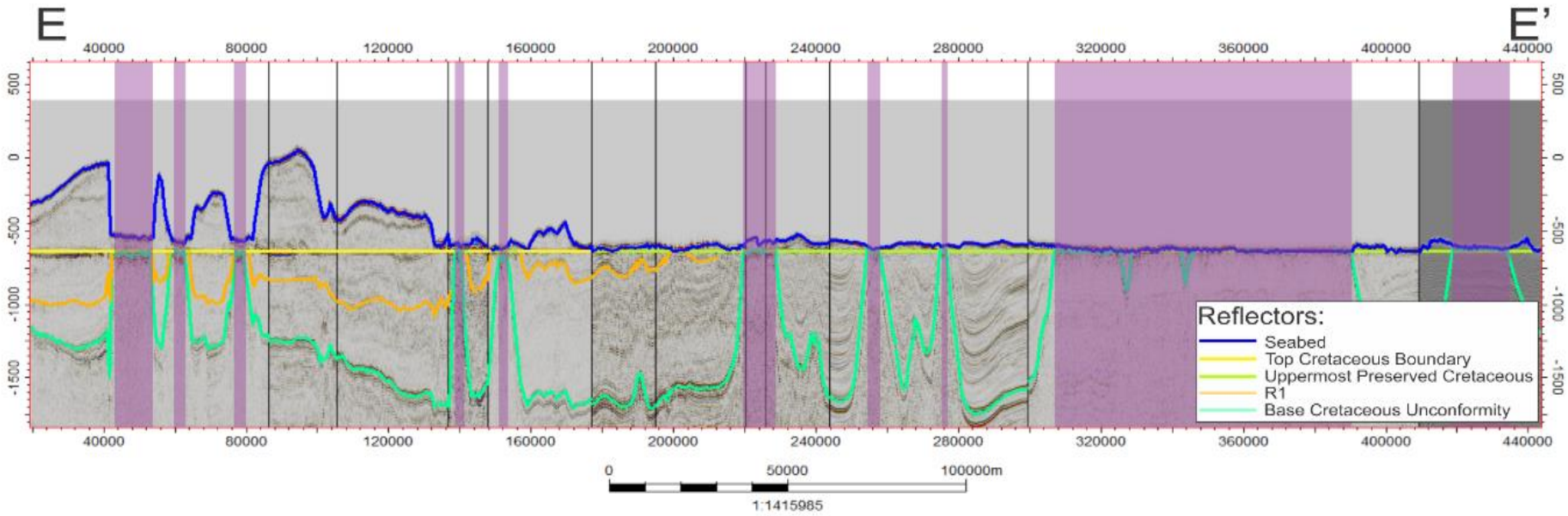

Figure 5.19: *Seismic profile EE' which is flattened according to the reflector of the Top Cretaceous Boundary and the Uppermost Preserved Cretaceous. Diapiric structures are highlighted with purple. Position of the profile is shown on the figure 5.10.*

5.3.4 Time-thickness of the Cretaceous succession

A time-thickness map generates between the Base Cretaceous Unconformity and the Top Cretaceous (or the uppermost preserved Cretaceous) and representing the Cretaceous in the Nordkapp Basin (figure 5.20), illustrates changes from 600 ms TWT to 1100-1200 ms TWT. The thickest intervals are located, where the sediments are not uplifted by salt diapirs. The thickness of the Cretaceous sequences increases from the margins of the basin. In the most areas of the basin, the Cretaceous time-thickness is in the interval between 900 and 1100 ms TWT, except the places, where the diapirs are present and in the southwest part of the Nordkapp Basin.

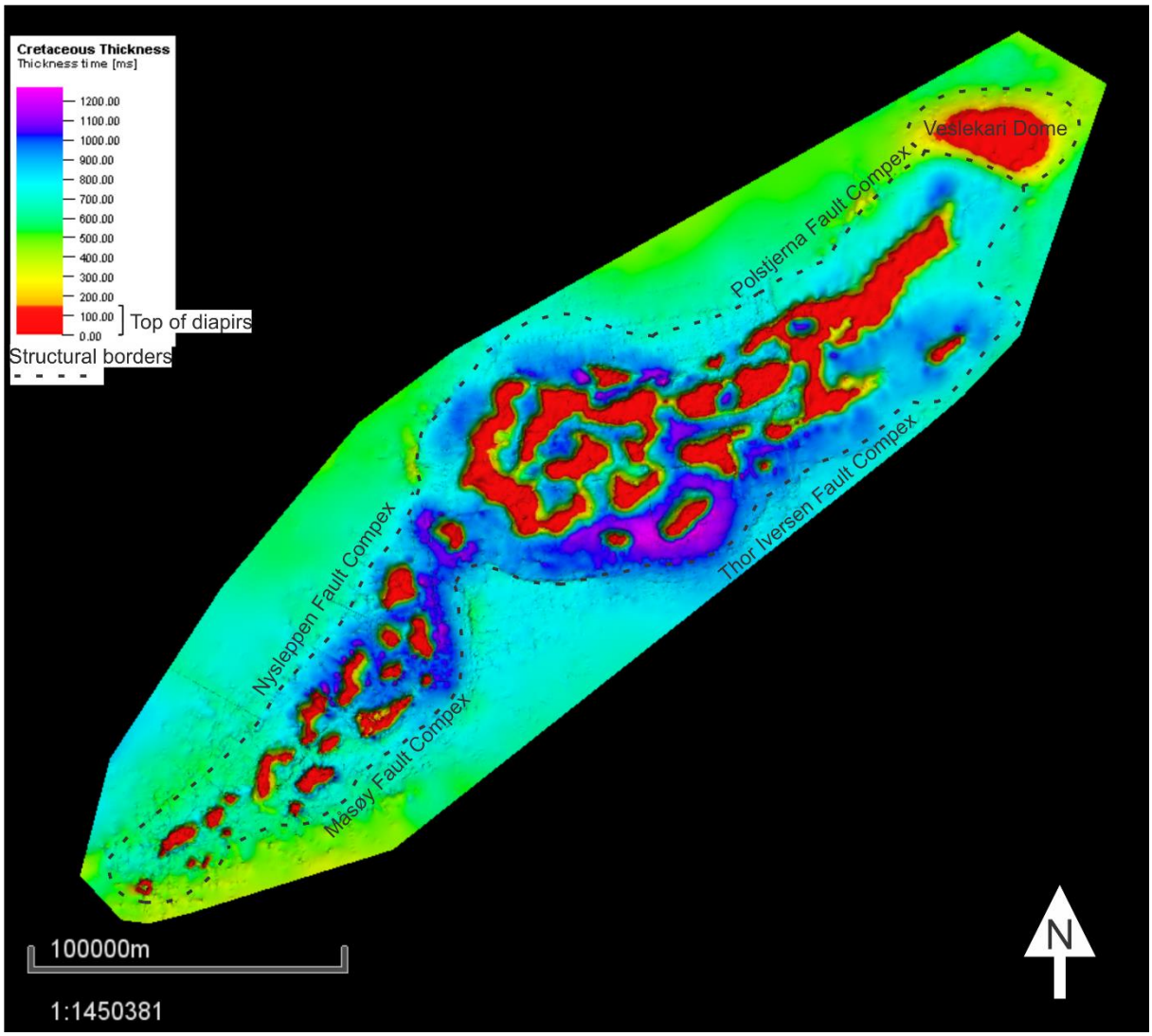

Figure 5.20: *Time-thickness map of the Cretaceous interval in the Nordkapp Basin and adjacent areas. Vertical exaggeration of 5 is used.*

The thinning in the southern part of the basin is due to different depth gradients of the Base and Top Cretaceous surfaces (figure 5.11, figure 5.15). This suggests the deposition change in the area. The Cretaceous thickness in this area varies between 700 and 800 ms TWT. The relatively sharp change in the slope and decrease in the time-thickness is also seen on the EE' profile near 100000 meters despite the interruption of layers by the salt diapirs (figure 5.11 and 5.15).

5.3.5 Time-thickness Top Cretaceous – R1 thickness

On the time-thickness map of the sequences between R1 and the Top Cretaceous Boundary the sediments which were not influenced by the Pliocene-Pleistocene erosion are easily noticeable (figure 5.21). The thickness of the sequences, deposited between these two seismic surfaces is uniform in the places, where the base Paleogene is present. The thickness of these sequences in the basin varies between 350 to 450 ms TWT. Outside the Nordkapp Basin variations in time-thickness are even less and are between 350 and 400 ms TWT. The uniformity in thickness inside the basin is due to the R1 and TCB reflectors are almost parallel to each other (section 5.3.2, 5.3.3) (figure 5.15, figure 5.16). Moreover, the reflectors between them also follow a parallel configuration pattern (section 2.1) which can be easily seen on seismic profiles (figure 5.11, figure 5.15, figure 5.16).

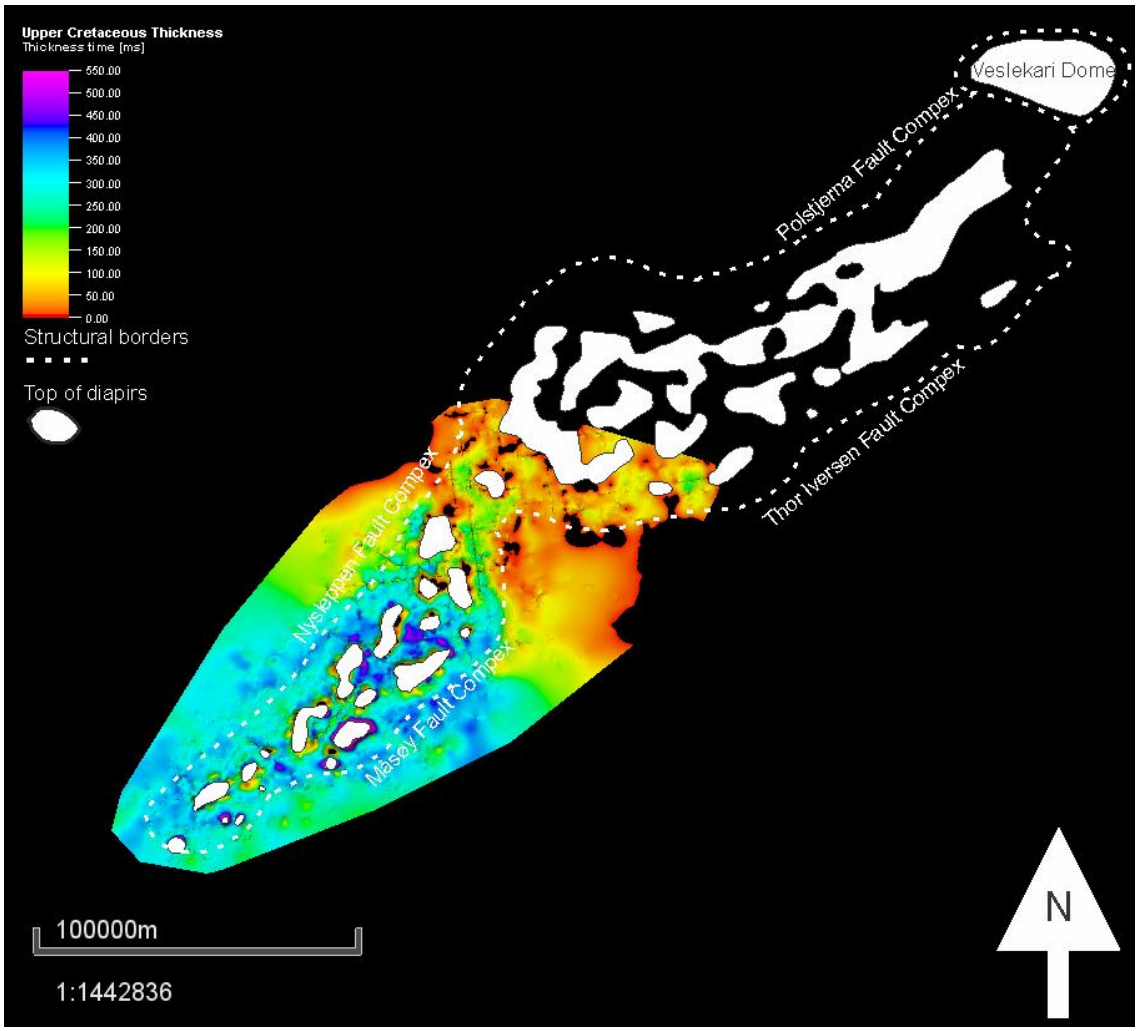

***Figure 5.21**: Time-thickness map of the interval between R1 horizon and the Top Cretaceous. Note that the base Paleogene was eroded in areas where the thickness is less than 250 ms and URU was used there in order to show the gradient. Vertical exaggeration of 5 is used.*

6. Discussion

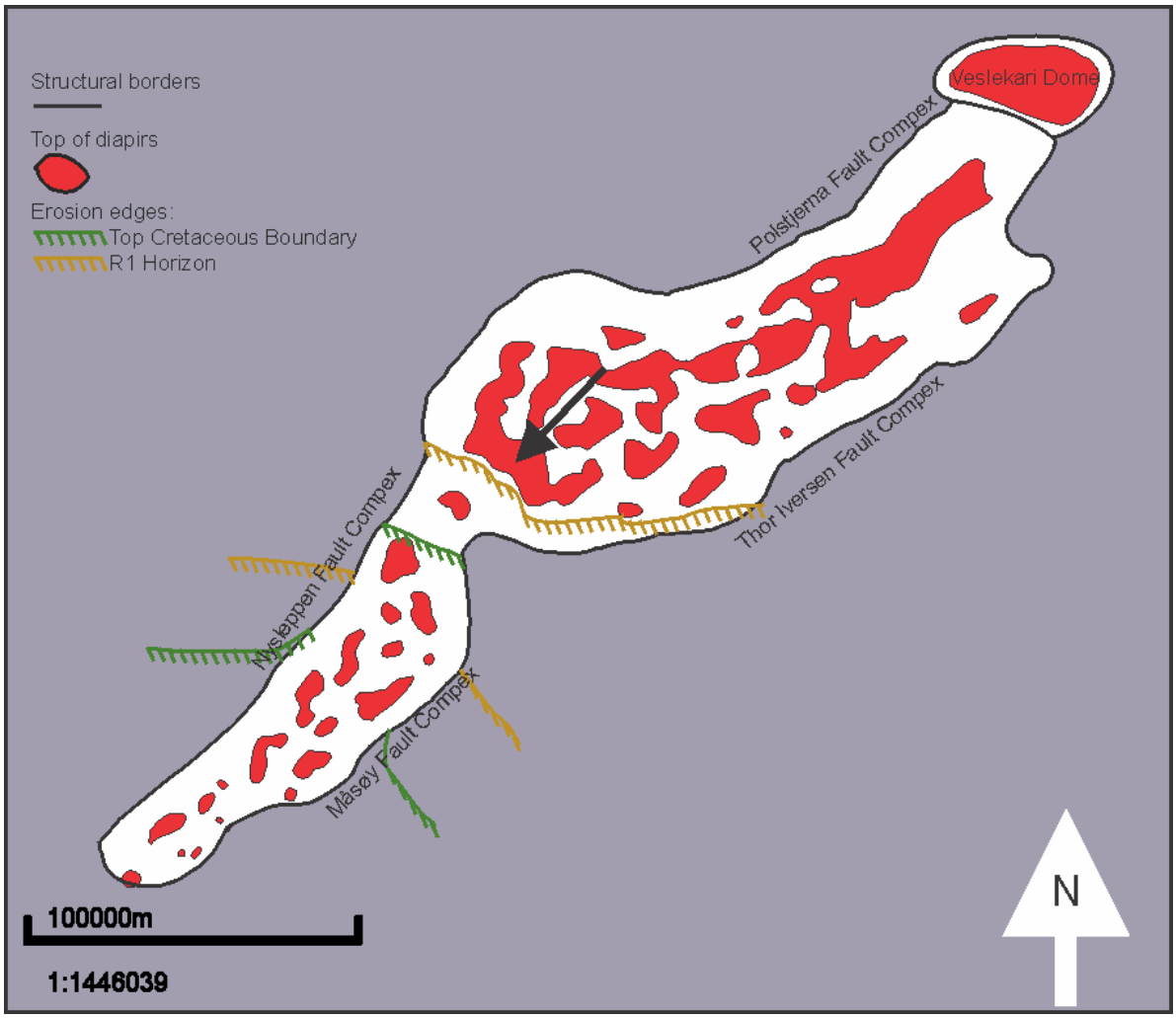

Figure 6.1: *A map of the Nordkapp Basin, showing salt diapirs and truncation boundaries of the seismic horizons R1 and the Top Cretaceous Boundary. Direction of slope progradation is shown with black arrow.*

6.1 Base Cretaceous Unconformity

The low relief of the BCU, described in section 5.3.1 (figure 5.14) can be explained by the model where the surface followed the overall trend of the region's gradient due to uplift in the northeast Barents Sea (figure 3.4, Smelror et al., 2009), during the Early Cretaceous and before salt diapirism occurred in the Nordkapp Basin. Fault complexes controlling the basin are clearly seen on the time-structure map (figure 5.14). The faults penetrate the Lower Cretaceous intervals, and it appears that the Lower Cretaceous sediments were deposited on the relatively smooth surface and the sharp borders of the basin were not present as today, due to lack of thickness differences across the faults. This, together with the findings made

during the analysis of the seismic profiles EE', FF', GG' (figures 5.11-5.13) (section 5.31), suggests that the development of faults as seen today delineating the Nordkapp Basin took place after generation of the Base Cretaceous Unconformity. The dip of the BCU from the flanks of the basin to its central parts, can be described by the fact that the basin already existed before the Cretaceous Period or subsided later. If there was a dip in the surface of the basin when the BCU was formed, then there most likely was a smoother slope on its flanks than now, due to later subsidence of the basin that has increased the present dip.

6.2 R1 horizon

The same faults which penetrate the BCU also penetrate R1 horizon (figure 5.13, figure 5.17) (section 5.3.1-5.3.2). The explanation of this can be that the north parts of the Nysleppen and the Masøy fault complexes were developed after R1 horizon was deposited. However, the major faults were not developed in the Lower Cretaceous sequences in the south parts of the fault complexes as much as in their north parts. Due to this, the gradient of the R1 horizon is smoother on the southern flanks of the Nordkapp Basin, than the gradient of the Base Cretaceous Unconformity surface in the same places.

As most of the other sequences and surfaces in the Nordkapp Basin, the R1 horizon was greatly affected by salt diapirism. The growth of the diapiric structures not only uplifted the horizon, but also caused the local subsidence of the reflector in the areas of the basin where the underlying Permian salts were moved from. The salt diapirism happened after the generation of the horizon, as the R1 horizon is seen uniform in the areas where the diapiric intrusions are not present and its depth is approximately the same on the different sides of the salt diapirs.

6.3 Top Cretaceous and its similarity to R1

Explanation of why the truncation line of the Top Cretaceous Boundary is at the same place, where the basin margins are (figure 5.18), can be that the fault complexes were also developed in the sedimentary layers, which were removed by the further Pleistocene-Pliocene erosion. The local subduction of the Cretaceous sediments in the southern part of the Nordkapp Basin preserved them from the erosion, which removed the same layers on the other side of the fault complexes.

As seen from the time-structure map (figure 5.18) (section 5.3.3), the Pliocene-Pleistocene erosion events removed the Upper Cretaceous sediments in the northeast part of the Nordkapp Basin. This makes mapping of the geological events in the area more difficult. However, due to preservation of the Upper Cretaceous sediments in the southwest part of the basin it is an evident, that the depth gradient of the Top Cretaceous Boundary is similar to the gradient of the R1 reflector (figure 5.18), suggesting that the surface was relatively smooth and inclined to the SW when was generated. Moreover, relative similarity of the dip of the Top Cretaceous (figure 5.18) and R1 (figure 5.17), and this also following the BCU trend (figure 5.14), suggests means that the salt structures did not affect sedimentation when these surfaces were formed. From this it is reasonable to suggest that the diapirs in the Nordkapp Basin raised through the Cretaceous layers in the Cenozoic and that salt tectonics remained inactive or was insignificant during the whole Cretaceous period.

Moreover, there is a sharp gradient on the time-thickness map of the Cretaceous succession in the southern part of the basin (figure 5.20) (section 5.3.4). This gradient indicates the potential of shelf slope in this area and its progradation towards the south. In the northern parts the thickness decreases from 1100 ms to 900 – 1000 ms TWT. This northward thinning in this part of the basin can be explained by glacial erosion of the Upper Cretaceous sediments and depth decrease of BCU surface (figure 5.14, figure 5.15). Moreover, a marine regression during the Cretaceous period due to uplift of the region to the north could influence the thickness of the sequences because of the shelf expansion and development of deltas farther out into the sea (figure 3.4, Smelror et al., 2009).

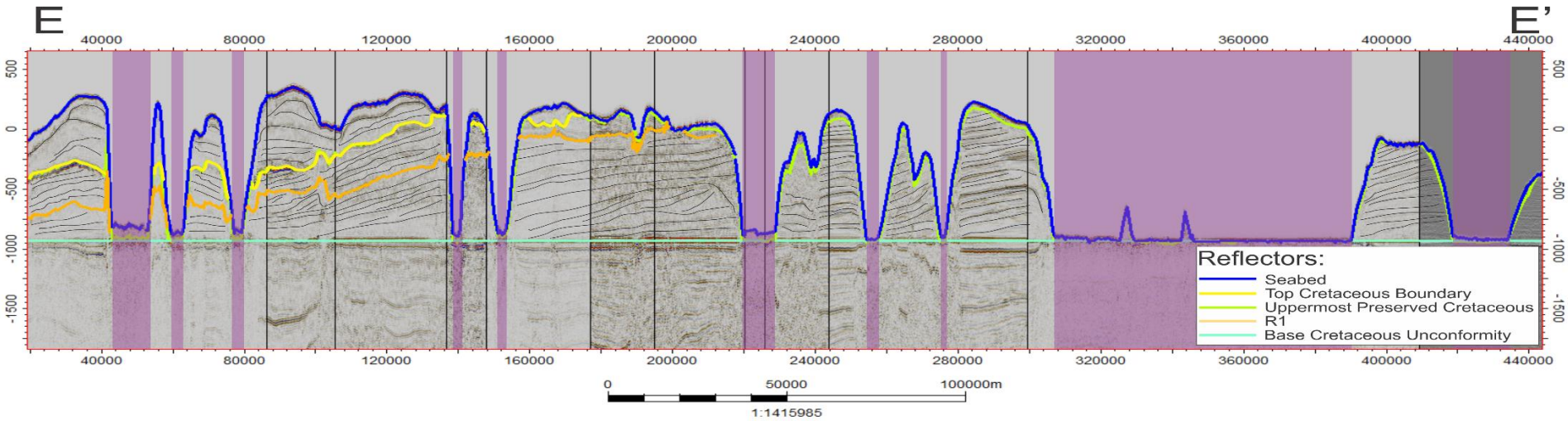

Figure 6.3: *Seismic profile EE' and seismic facies. The Profile is flattened according to the reflector of the Base Cretaceous Unconformity. Reflectors, which made configuration patterns are highlighted with black lines. Diapiric structures are highlighted with purple. Position of the profile is shown on the figure 5.10.*

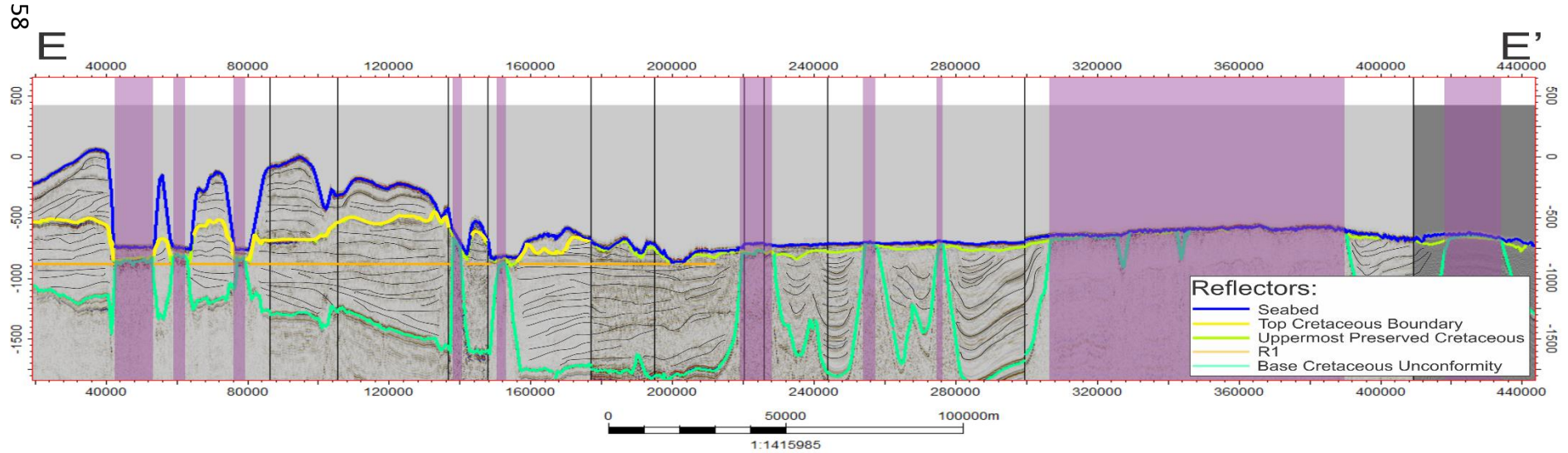

Figure 6.4: *Seismic profile EE' and seismic facies. The Profile is flattened according to the R1 reflector. Reflectors, which made configuration patterns are highlighted with black lines. Diapiric structures are highlighted with purple. Position of the profile is shown on the figure 5.10.*

6.4 The interval between R1 and the Top Cretaceous and its age.

It should be mentioned, that calling the sequences between the Top Cretaceous Boundary and R1 horizon as the Upper Cretaceous is inaccurate, as the R1 horizon was generated during the Albian Age (section 5.2) and does not correspond to top or base of the Albian Stage. According to this, the sequences which were deposited between the Top Cretaceous Boundary and R1 horizon were deposited during the Albian-Campanian ages and should not be included into the Upper Cretaceous sequences, as the Albian Age corresponds to the Early Cretaceous. Thus, it is more reasonable to call the sediments between R1 and Upper Regional Unconformity (in the middle of the basin, near the "bottleneck") as the Middle Cretaceous sediments, because they were deposited during Albian-Cenomanian ages, but there is no "Middle" epoch subdivision for the Cretaceous Period and the Cretaceous System according to the International Commission on Stratigraphy (ICS, 2017), and the term 'Upper' Cretaceous is applied with the above kept in mind.

The small difference in in the maximum time-thickness of non-eroded Albian-Campanian deposits inside and outside the Nordkapp Basin (450 and 400 ms TWT) (figure 5.21) (section 5.3.5) can be explained by the influence of the salt structures on the seismic survey inside the basin. The numerous distortions and lenses effect which are produced by the salt diapirs (section 4.3) can result in wrong appearance of the reflection occurring from near salt domes on the seismic profiles. Moreover, there are some salt structures or flanks of the diapirs, which did not penetrate the whole Cretaceous System, but only its lowest part (for example a salt structure between 100000 and 105000 meters on the seismic profile EE' (figure 5.11). Such structures also caused the uplift of the overlying layers and led to noise and distortion on seismic data, but their tops are not highlighted on the maps due to their deeper presence. The thickest parts of the Albian-Campanian deposits (those parts with thickness 350 ms TWT or more) are located on the flanks of the diapirs, so should not be considered as accurate data.

The negligible difference in the time-thickness intervals inside (350 – 450 ms TWT) and outside (300 – 400 ms TWT) the Nordkapp Basin in the places where there was no erosion can be also explained by the fact that the R1-TCB sequence is a little bit thicker inside of the basin than outside. This suggests that there could have been a small basin area along the middle axe of the present-day Nordkapp Basin. Such a small basin area could have been presented there

because of local subduction and fault development episodes in the Triassic-Jurassic periods in the Nordkapp Basin (Smelror et al., 2009; Mattos et al., 2016). This led to transport of sediments from flanks of the Nordkapp Basin to its middle axe. However, together with the diapiric distortions of the seismic signal described above, the maximum time-thickness difference is less than 50 milliseconds or 100 meters (section 4.2). As a result, the average time-thickness between R1 and TCB reflectors is just slightly bigger inside the basin than outside.

There are no large changes in the time-thickness map between the outer platforms and the basin in the areas, where there the base Paleogene is preserved. This indicates that the R1-TCB sequence was uniformly deposited and that the faults there were developed after the deposition of the sequence. Moreover, this further suggests that the diapiric structures in this area remained inactive at least during the Albian and Cenomanian ages.

6.5 Salt movements and developments during the Cretaceous Period

The analysis and discussion of the constructed maps showed that the marginal faults along the borders of the Nordkapp Basin influence the Triassic, whole Jurassic and Cretaceous layers and were developed after the deposition of the whole Cretaceous sequence. (section 5.3.1 – 5.3.3, 6.1-6.4) (figure 5.14, figure 5.17 and figure 5.18).

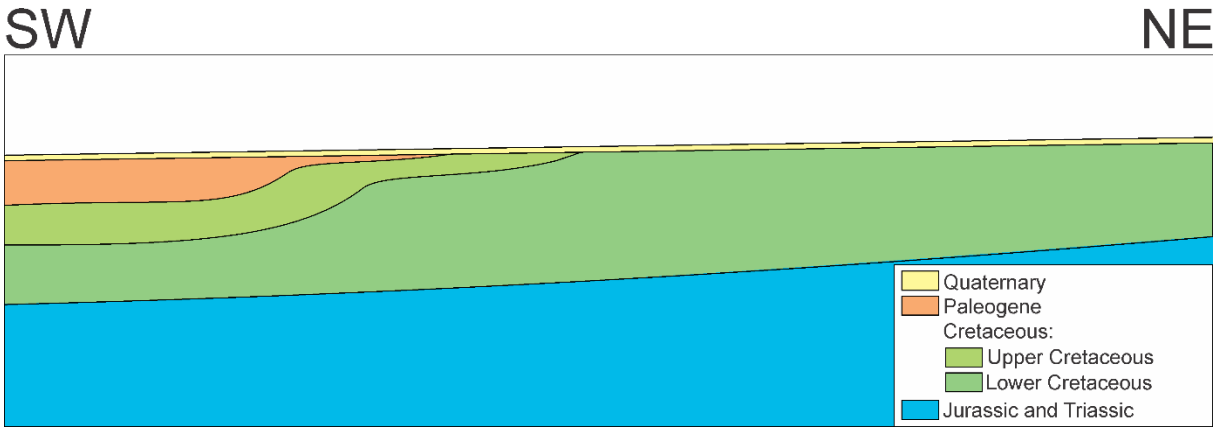

Figure 6.2: *A sketch showing hypothetical model of the Nordkapp Basin without diapiric structures and with the general pattern of the Cretaceous sequences. The sketch is made along the basin approximately at the same place as EE' profile. Note, that this sketch includes the erosion events of the Paleogene and Neogene periods.*

Diapirs in the basin are elongated to rounded / sub-rounded along the central axis of the basin. The diapirs appears to change their orientation when the central axe of the basin changes its direction. This is illustrated on the map of the Nordkapp Basin (figure 6.1). Moreover, the diapirs in the northeast part of the basin are wider, than the diapirs in the southwest part of it (figure 6.1). The explanation of this can be that the southwest part of the Nordkapp Basin is generally narrower than the northeast part which led to deposition of the smaller amount of salt there, compared to the northeast part. As a result, the diapiric structures in the southwest part of the basin follows the pattern of the structures in the northwest part, but are narrower possible due to less salt, and / or different and less space to develop in a narrower basin.

The equal thicknesses of the deposition of the Cretaceous Layers described above (section 6.1-6.4), suggest that there were no salt movements at least in the southwest part of the basin during the Cretaceous Period. However, timing of the second phase of the halokinesis in the northwest part of the basin is complicated, because even Albian layers were removed in this area by massive erosion (the first phase of halokinesis happened in the Early Triassic Period (section 3.3) (Dengo et al., 1992; Jensen et al., 1992; Halland et al., 2014)). In the preserved Lower Cretaceous layers there are no evidences of growth of the diapirs during the time of deposition of these layers.

The Paleocene – Early Eocene continental break up along the North Atlantic Ridge could be an event which triggered the fault development along the borders of the Nordkapp Basin in the Cretaceous (section 3.2) (Faleide et al., 1996). Moreover, this rifting in the west together with continued deposition and increase of weight of overlying sediments in the Nordkapp Basin area could booster the development of the diapirs in the basin. The growth of salt structures led to uplift of the sedimentary layers which were overlying the diapirs and subsidence of sediment where the salt was removed from. This subsidence could have been associated with fault movements along the flanks of the Nordkapp Basin (figure 6.1). The initial fault movements on the flanks of the Nordkapp Basin could have been the primary result of the rifting in the west, but the further subsidence happened due to salt tectonics and could have increased the fault development as salt structures continued to grow. However, there are no evidences that the marginal faults in the southwest part of the basin (Nysleppen and Måsøy fault complexes) and marginal faults of the northeast part of the basin (Thor Iversen and Polstjerna fault complexes) were developed simultaneously.

The difference in location of the erosion boundaries of seismic horizons TCB and R1 inside and outside the Nordkapp Basin (figure 6.1) is due to post-Cretaceous subsidence of the basin relative to the surrounding areas, and erosion of near 1200 meters of overlying sediments (Dengo et al., 1992; Faleide et al., 1996; Smelror et al., 2009). As it was mentioned above (section 5.3.4, 6.3-6.4) R1, TCB and the reflectors between them are parallel to each other (figure 6.3). In addition to the reflectors between R1 and TCB horizons, there are also seen clinoform patterns below R1 horizon. It is still difficult to describe the nature and style of Cretaceous clinoforms in the Nordkapp Basin because of later diapiric intrusions and erosion, but the general pattern and average inclination of the reflectors can be seen (figure 6.3, figure 6.4). If there is assumed that there were not any salt movements also in the north part of the basin during the Cretaceous Period, then the shelf was prograding uniformly in the southwest direction without any disturbance. The hypothetical appearance of the discussed Cretaceous sequences, if there had never been any diapirs, is shown on the model along the Nordkapp Basin (figure 6.2).

Moreover, it is seen that most of the deposition in the basin during the Cretaceous Period, happened between the Aptian – Mid Cenomanian ages. This is indicated by well data, which show, that the Kolje Formation is not present in the wells used in this thesis (section 4.2). This formation was deposited during the Barremian – Early Aptian (NDP, 2017c). Moreover, the Knurr Formation which is thinning to the north and is present in some wells, also is truncated in areas north to the middle part of the basin (the basin's ''bottleneck'', which divides north and south parts). The age of the formation corresponds to Valanginian – Barremian. This, together with the seismic data, indicates the lack of sedimentation during the Late-Jurassic – Early Cretaceous (before the Aptian Age) (figure 6.5A), and is represented as the Base Cretaceous Unconformity. The thick sequences of Lower Cretaceous were deposited during the shelf progradation (figure 6.5B). The sediments were transported by river systems from the northeast part of the Barents Sea (the High Arctic Large Igneous Province), which was tectonically active during the Cretaceous (Smelror et al., 2009). The thinner Upper Cretaceous sequences continued to follow the general pattern of deposition while the salt tectonics was inactive (figure 6.5C). The continental break-up in the Paleogene (Paleocene – Eocene epochs), reactivated the salt movements and development of faults (figure 6.5D). The diapiric growth led to further subduction of the sediments on the flank of the basin and their uplift in

places near and above the diapirs (6.5E). It is not straightforward to suggest how the Paleogene sequences and the diapirs looked like due to later erosion, but the whole region was uplifted and the erosion of the upper layers probably started in the Late Paleogene Period. The further glacial erosion in the Pliocene-Pleistocene led to removal of the Paleogene and Upper Cretaceous sediments and led to formation of the Upper Regional Unconformity (figure 6.5F).

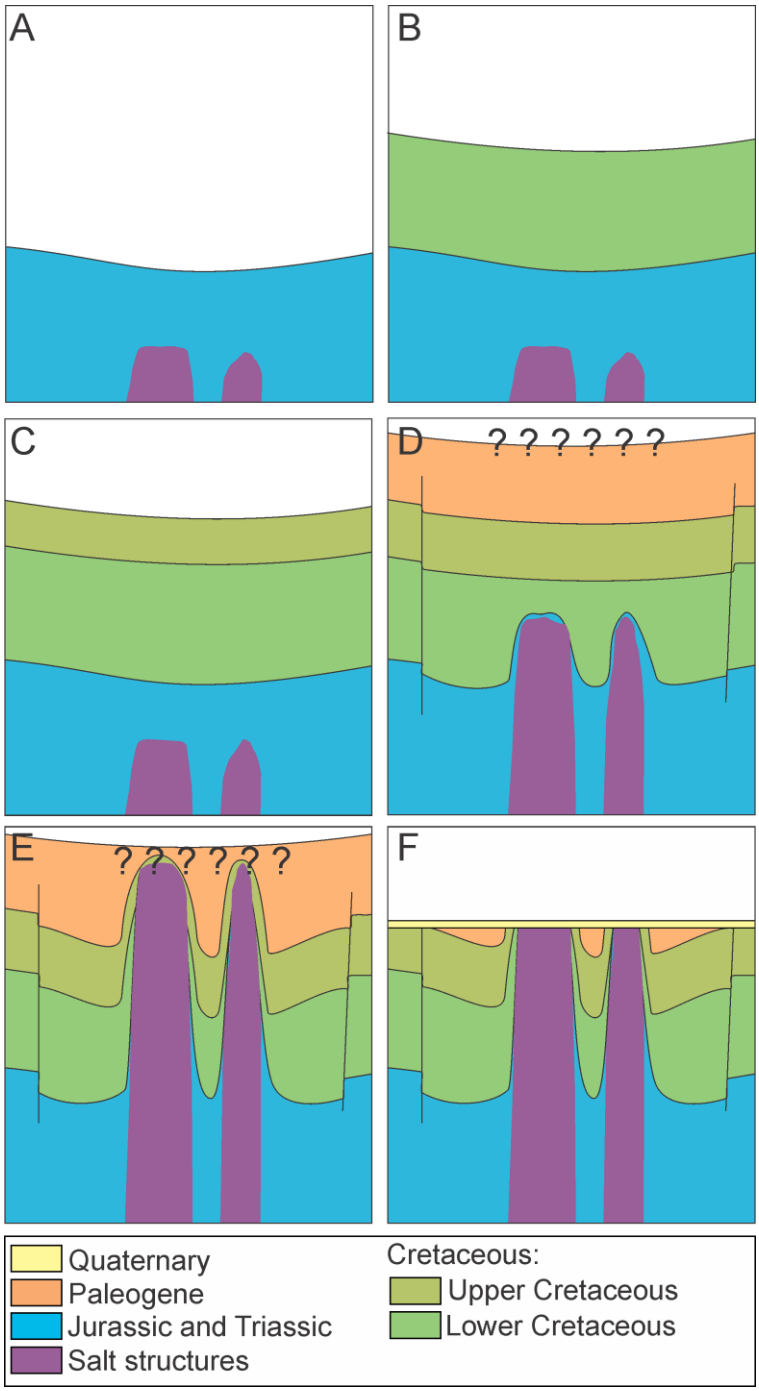

Figure 6.5: *Sketches, showing the development of the Nordkapp Basin after the Jurassic Period.* **A:** *Late Jurassic - Early Cretaceous (Berrasian). Lack of the sedimentation and erosion.* **B:** *Early Cretaceous (Berrasian – Albian)* **C:** *Late Cretaceous. Deposition of thinner sequences.* **D:** *Paleocene – Early Eocene epochs of Paleogene. Start of diapiric growth and faulting.* **E:** *Late Paleogene – Neogene. Development of salt diapirs and faults.* **F:** *Neogene - Quaternary. Massive erosion and formation of the Upper Regional Unconformity.*

7. Summary and conclusion

During this work, the geological evolution of the Nordkapp Basin in the Cretaceous Period was studied. The two main reflectors were interpreted and analysed: the Base Cretaceous Unconformity (BCU) and the Top Cretaceous Boundary (TCB). The Base Cretaceous Unconformity reflector corresponds to the base of the Knurr Formation in places where it is present or the base of the Kolmule Formation. The Top Cretaceous Boundary is related to the top of the Kviting Formation in places, where the Upper Cretaceous was not removed by the Cenozoic erosion events. In the other areas, the Upper Cretaceous is truncated by the Upper Regional Unconformity. In addition to the BCU and the TCB, a less prominent reflector R1 was interpreted. Seismic to well correlation showed that age of this horizon corresponds to the Albian. Construction of the time-structure map of the Base Cretaceous, the Top Cretaceous, R1 and the associated time-thickness maps helped to understand the development of the basin during the Cretaceous Period. Similarity of R1 and the TCB reflectors repeatedly showed the uniform deposition of the Cretaceous sequences. Moreover, analysis of all the interpreted reflectors showed more evidences of shelf progradation from NE to SW along the basin.

The regional evolution of the Barents Region directly influenced the development of the Nordkapp Basin. Regional uplift in the north part of the sea and the following southward deltaic transport of terrigenous material in the Cretaceous period (Smelror et al., 2009) led to deposition of thick sequences of clastic sediments in the area. During the period salt tectonics was not active in the Nordkapp Basin. The major marginal faults delineating the Nordkapp Basin appear not have been active in the Cretaceous. The shelf was prograding from NE to the SW along the Nordkapp Basin without any interruptions and disturbances. There could have been a small basin area, possibly less than 100 meters deep at its deepest point, which went along the middle axe of the present-day Nordkapp Basin (section 6.4). However, it seems that the Nordkapp Basin was not developed as a major structural basin during the Cretaceous Period.

The Cretaceous Period for the Nordkapp Basin was marked by high rates of deposition followed the uplift in the northeast Barents Region and inactive faulting and halokinesis. The rifting events in the North Atlantic and opening of the Barents Sea in the Early Paleogene (Faleide et al., 1984, Breivik et al., 1998) reactivated the upward movement of salt and fault

development in the Nordkapp Basin. These, together with further glacial erosion, dramatically changed the appearance of the basin.

8. References

Andreassen, K., 2009. Marine Geophysics. Lecture Notes for Geo-3123. Tromsø: UiT.

American Association of Petroleum Geologists (AAPG), 2017. Province, basin, system, play, and prospect. AAPG Wiki. Date accessed 9 December 2017. http://wiki.aapg.org/Province,_basin,_system,_play,_and_prospect

Bjoroy, M., Hall, P.T., Ferriday, I.L., Mork, A., 2009. Triassic Source Rocks of the Barents Sea and Svalbard. Search and Discovery Article #10219, AAPG Convention, Denver, Colorado, June 7-10, 2009

Bourbié, T., Coussy, 0., Zinszner, B., 1987. Acoustics of Porous Media, Gulf Publishing Company, Book Division, ISBN: 978-0-8720-1025-3

Breivik, A.J., Gudlaugsson, S.T., Faleide, J.I., 1995. Ottar Basin, SW Barents Sea: a major Upper Palaeozoic rift basin containing large volumes of deeply buried salt. Basin Research 7, 299–312.

Breivik, A.J., Gudlaugsson, S.T., Faleide, J.I., 1998. Southwestern Barents Sea margin: late Mesozoic sedimentary basins and crustal extension. Basin Research 293, 21-44.

Bugge, T., Elvebakk, G., Fanavoll, S., Mangerud, G., Smelror M., Weiss, H.M, Gjelberg J., Kristensen, S.E., Nilsen, K., 2002. Shallow stratigraphic drilling applied in hydrocarbon exploration of the Nordkapp Basin, Barents Sea. Marin and Petroleum Geology, 19 (1), 13-37. doi 10.1016/S0264-8172(01)00051-4

Dengo C.A., K.G. Røssland, 1992. Extensional tectonic history of the western Barents Sea. Structural and Tectonic Modelling and its Application to Petroleum Geology by Larsen R.M., Brekke H., Larsen B.T. and Talleraas E.,1992, 91-107, ISBN: 0-44-88607-9

Doré. A., 1995. Barents Sea geology, petroleum resources and commercial potential, Arctic, 48 , 207-221

Faleide J.I., Gudlaugsson, S. T., Gerard Jacquart G., 1984. Evolution of the western Barents Sea, Marine and Petroleum Geology, vol 1, Issue 2, 128-150. doi:10.1016/0264-8172(84)90082-5

Faleide, J.I., Solheim, A., Fiedler, A., Hjelstuen, B.O., Andersen, E.S., Vanneste, K, 1996. Late Cenozoic evolution of the western Barents Sea–Svalbard continental margin. Glob. Planet. Chang. (1996), 10.1016/0921-8181(95)00012-7

Faleide, J.I., Vågnes, E., Gudlaugsson, S.T., 1993. Late Mesozoic–Cenozoic evolution of the south-western Barents Sea in a regional rift-shear tectonic setting. Marine and Petroleum Geology, 10, 186-214

Gernigon L., Brönner, M., 2011. Late Palaeozoic architecture and evolution of the southwestern Barents Sea: insights from a new generation of aeromagnetic data. Geological Survey of Norway, 2011.076, ISSN 0800-3416
http://www.ngu.no/upload/Publikasjoner/Rapporter/2011/2011_067.pdf

Gradstein, F., Ogg, J., & Smith, A., 2004. A Geological Time Scale 2004. Camebridge University Press 2004, 344-383, ISBN 0521-78142-6

Halland E.K., Bjørnestad A., Gjeldvik, I.T., Bjørheim, M., Magnus, C., Mujezinović, J. & others, 2014. Barents Sea. CO2 Storage Atlas, NPD. 108-145

Hanania J., Stenhouse K., Donev, J., 2016. Oil and gas traps. Energy Education. Date accessed September 17, 2017 http://energyeducation.ca/encyclopedia/Oil_and_gas_traps

International Commission on Stratigraphy (ICS) 2017. International Chronostratigraphic Chart. Date accessed September 11, 2017 http://www.stratigraphy.org/index.php/ics-chart-timescale

Jablonski, D., Chaloner, W. G., 1994. Extinctions in the fossil record (and discussion). Philosophical Transactions of the Royal Society of London, Series B. 344 (1307): 11–17. doi:10.1098/rstb.1994.0045

Jensen L.N., Sørensen K., 1992. Tectonic framework and halokinesis of the Bordkapp Basin, Barents Sea. Structural and Tectonic Modelling and its Application to Petroleum Geology by Larsen R.M., Brekke H., Larsen B.T. and Talleraas E.,1992, 109-120, ISBN: 0-44-88607-9

Jones, I.F., Davison I., 2014. Seismic imaging in and around salt bodies. SEG, Interpretation, 2(4), SL1-SL20. https://doi.org/10.1190/INT-2014-0033.1

Jones, K. & Blake, S., 2003. Mountain building in Scotland, 47–50, ISBN 0-7492-5847-0

Kring, D. A., 1995, The dimensions of the Chicxulub impact crater and impact melt sheet, J. Geophys. Res., 100(E8), 16979–16986, doi:10.1029/95JE01768

Magoon, L.B, Beaumont, E.A., 1999. Treatise of Petroleum Geology. Handbook of Petroleum Geology: Exploring for Oil and Gas Traps. 3-34

Marin, D., Escalona, A., Sliwinska, K.K., Nøhr-Hansen, H., Mordasova, A., 2017. Sequence stratigraphy and lateral variability of Lower Cretaceous clinoforms in the southwestern Barents Sea.

Marshak S., 2012, Essentials of Geology. W. W. Norton & Company, 4th edition, ISBN: 978-0393919394

Mattingsdal, R., Høy, T., Simonstad, E., Brekke, H., 2015. An updated map of structural elements in the southern Barents Sea

Mattos, N.H., Alves T.M., Omosanya K.O., 2016. Crestal fault geometries reveal late halokinesis and collapse of the Samson Dome, Northern Norway: Implications for petroleum systems in the Barents Sea, Tectonophysics, vol. 690, Part A, 76-96. doi:10.1016/j.tecto.2016.04.043

Mitchum, R.M., Vail P.R., Sangree J.B., 1977. Seismic stratigraphy and global changes in sea level, part 6: stratigraphic interpretations of seismic reflection patterns in depositional sequences, in Payton, C., E., ed., Seismic Stratigraphy and Applications to Hydrocarbon Exploration: AAPG Memoir 26, p. 117–133.

Nichols, G., 2009. Sedimentology and stratigraphy. Wiley-Blackwell; 2 edition (2009), 278, ISBN 978-1-4051-3592-4

NPD, 2014a. The 2014 NPD lithostratigraphic charts. Date accessed September 23, 2017 http://www.npd.no/en/Topics/Geology/Lithostratigraphy/

NPD, 2014b. Geology of the Barents Sea. Date accessed November 11, 2017 http://www.npd.no/en/Publications/Reports/Compiled-CO2-atlas/6-The-Barents-Sea/61-Geology-of-the-Barents-Sea/

NPD, 2017a. Fact Map wms service. Date accessed September 14, 2017 http://gis.npd.no/ogc/factmaps/2_0

NPD., 2017b. Geological plays. Date accessed September 13, 2017 http://www.npd.no/en/topics/geology/geological-plays/

NPD, 2017c. Fact-pages of Exploration Wellbores. Date accessed October 10, 2017 http://factpages.npd.no/

Peacock, D., Nixon, C., Rotevatn, A., Sanderson, D., & Zuluaga, L., 2016. Glossary of fault and other fracture networks. Journal of Structural Geology, 92, 12-29. doi:10.1016/j.jsg.2016.09.008

Press, F., Siever, R., 1994. Understanding Earth. W.H. Freeman and Company, 51

Ramberg, I.B., Bryhni, I., Nøttvedt, A., Rangnes, K., 2008. The Making of a Land: Geology of Norway. Norwegian Geological Society, ISBN 978-82-92-39442-7

Selley, R.C., Sonnenberg S.A., 2014. Elements of Petroleum Geology, 3ed, Academic Press, ISBN 978-01-23-86031-6

Sheriff, R.E., 2006. Encyclopedic Dictionary of Exploration Geophysics, 5, Society of Exploration Geophysics.

Smelror, M., Petrov, O., Larssen, G. B. & Werner, S. 2009. Atlas. Geological history of the Barents Sea. Geological Survey of Norway. ISBN 978-82-7385-137-6

Sosiety of Exploration Geophysicists (SEG), 2017. Seismic resolution. SEG Wiki. Date accessed 10 December 2017. https://wiki.seg.org/wiki/Seismic_resolution

Stoneley, R., 1995. North Sea petroleum plays. Introduction to Petroleum Exploration for Non-geologists. Oxford University Press, 106. ISBN 0-19-854856-7

TGS, 2017. Geophysical Data Catalog. Date accessed 10 oct. 2017 http://www.tgs.com/products-and-services/geophysical/data-catalog/europe/europe-northern/bare-02/

Trusheim, F., 1960. Mechanism of Salt Migration in Northern Germany. AAPG Bulletin, 44. doi:10.1306/0bda61ca-16bd-11d7-8645000102c1865d

Vendeville, B. C., 2002. A new interpretation of Trusheim's classic model of salt-diapir growth.

Wernicke, B., 1981. Low-angle normal faults in the Basin and Range Province: nappe tectonics in an extending orogen. Nature. 291 (25): 645–648. doi:10.1038/291645a0

Yilmaz, Ö., 2001. Investigations in Geophysics. Seismic Data Analysis: Processing, Inversion, and Interpretation of Seismic Data. SEG. ISBN: 978-1-56080-094-1